High precision computation of the distance between the invariant manifolds of L_3 in the RPC3BP

Ernesto Lanchares Sánchez

Advisors

Inmaculada Baldomà Barraca   Mercè Ollé Torner

UNIVERSITAT POLITÈCNICA DE CATALUNYA
BARCELONA**TECH**
Facultat de Matemàtiques i Estadística

June 21, 2022

Abstract

Recently an asymptotic formula for the distance of the invariant manifolds of L_3 in the RCP3BP when the mass parameter tends to zero was proven. In this study we numerically check the formula using high precision routines and give approximate values for the constants involved.

keywords: *invariant manifold, Parameterization method, inner equation*

Resumen

Recientemente, se ha demostrado una fórmula asintótica para la distancia entre las variedades invariantes del punto L_3 en el problema RCP3BP cuando el parámetro de masas tiende a cero. En este estudio vamos a comprobar numéricamente esta fórmula utilizando métodos de alta precisión y aproximaremos valores para las constantes involucradas.

palabras clave: variedad invariante, método de la parametrización, ecuación inner

MSC2020: 34, 37

4

Resum

Recentment, s'ha demostrat una fórmula asimptòtica per a la distància entre les varietats invariants del punt L_3 en el problema RCP3BP quan el paràmetre de masses tendeix a zero. En aquest estudi comprovarem numèricament aquesta fórmula utilitzant mètodes d'alta precisió i aproximarem valors per a les constants involucrades.

paraules clau: varietat invariant, mètode de la parametrització, equació inner

Acknowledgements

First of all, I would like to express my gratitude to both Inmaculada Baldomà and Mercè Ollé for their time, guidance, and support during these months. This thesis would not have been possible without their advice and knowledge. I would like to thank them for their time and dedication specially outside working hours when the programs described in this thesis were not working.

Contents

Chapter 1

Introduction

This thesis is concerned with the Restricted Circular Planar Three Body Problem or RCP3BP for short. Let us give a brief history of how the problem naturally arises when considering celestial dynamics.

Suppose that you want to send a satellite to a system of two bodies. This will usually mean two massive planets or stars. You will need a system of ODEs that describes the motion of your spacecraft in order to make the necessary computations in the trajectory and velocity of the satellite. As is usual, you decide to neglect the gravitational forces applied by either far away or less massive objects and only consider the forces from the two bodies. Most real scenarios are considering artificial satellites in the system of the Earth and the Moon and natural satellites in the system of Jupiter and the Sun.

Using Newton's equations, you obtain the system

$$m_1 \ddot{q}_1 = G \frac{m_1 m_2}{\|q_1 - q_2\|^3}(q_2 - q_1) + G \frac{m_1 m_S}{\|q_S - q_1\|^3}(q_S - q_1)$$
$$m_2 \ddot{q}_2 = G \frac{m_2 m_1}{\|q_1 - q_2\|^3}(q_1 - q_2) + G \frac{m_2 m_S}{\|q_S - q_2\|^3}(q_S - q_2)$$
$$m_S \ddot{q}_S = G \frac{m_S m_1}{\|q_1 - q_S\|^3}(q_1 - q_S) + G \frac{m_S m_2}{\|q_2 - q_S\|^3}(q_2 - q_S),$$

where m_1, m_2, q_1, q_2 are the mass and positions with respect to some fixed origin of the two massive bodies (that we will call primaries) and m_S, q_S are the ones from your spacecraft or small satellite (which we call secondary). After dividing each equation by m_1, m_2 and m_S respectively, we obtain the

equivalent system

$$\ddot{q}_1 = G\frac{m_2}{\|q_2 - q_1\|^3}(q_2 - q_1) + G\frac{m_S}{\|q_S - q_1\|^3}(q_S - q_1)$$
$$\ddot{q}_2 = G\frac{m_1}{\|q_1 - q_2\|^3}(q_1 - q_2) + G\frac{m_S}{\|q_S - q_2\|^3}(q_S - q_2) \qquad (1.1)$$
$$\ddot{q}_S = G\frac{m_1}{\|q_1 - q_S\|^3}(q_1 - q_S) + G\frac{m_2}{\|q_2 - q_S\|^3}(q_2 - q_S).$$

Since the mass of the secondary (by the nature of the problem) is really small in comparison to the ones of the primaries ($m_s << m_1, m_2$) we consider it insufficient to disturb the orbit of either of the primaries. For that reason we decide to ignore its contribution to the motion of the primaries, i.e. we neglect the contribution of the secondary and consider the system (1.1) with $m_S = 0$

$$\ddot{q}_1 = G\frac{m_2}{\|q_2 - q_1\|^3}(q_2 - q_1)$$
$$\ddot{q}_2 = G\frac{m_1}{\|q_1 - q_2\|^3}(q_1 - q_2)$$
$$\ddot{q}_S = G\frac{m_1}{\|q_1 - q_S\|^3}(q_1 - q_S) + G\frac{m_2}{\|q_2 - q_S\|^3}(q_2 - q_S).$$

Presumably one does know the motions of the two primaries in advance and with a high degree of precision so we are left with the second order ODE

$$\ddot{q}_S = G\frac{m_1}{\|q_1(t) - q_S\|^3}(q_1(t) - q_S) + G\frac{m_2}{\|q_2(t) - q_S\|^3}(q_2(t) - q_S).$$

When the two bodies are in an elliptic orbit with small eccentricity, it is often good enough to consider that the two primaries are in circular orbits around the common center of mass. This happens in the Jupiter-Sun system or the Earth-Moon system. Assume also that we restrict the movement of the secondary to the plane of motion of the two primaries. Then we can take coordinates around the center of mass of the primaries such that their motions are described by

$$\begin{cases} q_1(t) = \mu\left(\cos(\omega t), \sin(\omega t)\right) \\ q_2(t) = (\mu - 1)\left(\cos(\omega t), \sin(\omega t)\right) \end{cases}$$

where we have assumed without loss of generality that $m_1 \geq m_2$ and $\mu = \frac{m_2}{m_1 + m_2} \in [0, 0.5]$ is the mass parameter. Now, it is trivial to take rotating coordinates, also called synodic coordinates, such that the positions of

the primaries are fixed at points $(\mu, 0)$ and $(\mu - 1, 0)$. In this coordinate system, the dynamics of the secondary body are described by the Hamiltonian system given by Hamiltonian

$$H(q, p) = \frac{\|p\|}{2} - q^t \begin{pmatrix} 0 & 1 \\ -1 & 0 \end{pmatrix} p - \frac{1 - \mu}{\|q - (\mu, 0)\|} - \frac{\mu}{\|q - (\mu - 1, 0)\|} \quad (1.2)$$

with $q = (q_x, q_y)$, $p = (p_x, p_y) = (\dot{q_x} - q_y, \dot{q_y} + q_x)$ and we have dropped the subindices avoiding a cumbersome notation. The equations of motion associated with (1.2) are

$$\begin{cases} \dot{q_x} = \partial_{p_x} H(q, p) = p_x + q_y \\ \dot{q_y} = \partial_{p_y} H(q, p) = p_y - q_x \\ \dot{p_x} = -\partial_{q_x} H(q, p) = p_y + \frac{(1-\mu)(\mu - q_x)}{\left((\mu - q_x)^2 + q_y^2\right)^{\frac{3}{2}}} + \frac{\mu(\mu - q_x - 1)}{\left((\mu - q_x - 1)^2 + q_y^2\right)^{\frac{3}{2}}} \\ \dot{p_y} = -\partial_{q_y} H(q, p) = -p_x - q_y \left[\frac{1 - \mu}{\left((\mu - q_x)^2 + q_y^2\right)^{\frac{3}{2}}} + \frac{\mu}{\left((\mu - q_x - 1)^2 + q_y^2\right)^{\frac{3}{2}}} \right]. \end{cases} \quad (1.3)$$

This is a widely studied system and some of its properties are well known. Here we will describe some of them. We leave most of the proofs out as they are more involved but we provide references so any interested reader can go and check the proofs by themselves.

One can note that (see [MO17]) the system has a symmetry in the equations

$$(q_x, q_y, p_x, p_y; t) \leftrightarrow (q_x, -q_y, -p_x, p_y; -t). \quad (1.4)$$

Meaning that for every solution "forwards in time" (namely $t \geq 0$)

$$(q_x(t), q_y(t), p_x(t), p_y(t)),$$

we have a solution that is symmetric with respect to the plane $\{q_y = 0, p_x = 0\}$ but runs "backwards"

$$(q_x(-t), -q_y(-t), -p_x(-t), p_y(-t)), \quad t \geq 0.$$

In other words, in the configuration space (q_x, q_y), the trajectory is symmetric with respect to $q_y = 0$ with tangent vector $(\dot{q_x}, \dot{q_y})$.

Also, the system has 5 equilibrium points L_1, L_2, L_3, L_4 and L_5, the celebrated Lagrange points. Their relative position with respect to the primaries can be visualised in Figure 1.1. The points L_4 and L_5 are called the triangular Lagrange points because they form an equilibrium triangle with the two primaries. And L_1, L_2 and L_3 are called the collinear Lagrange points because they are located in the same line as the primaries
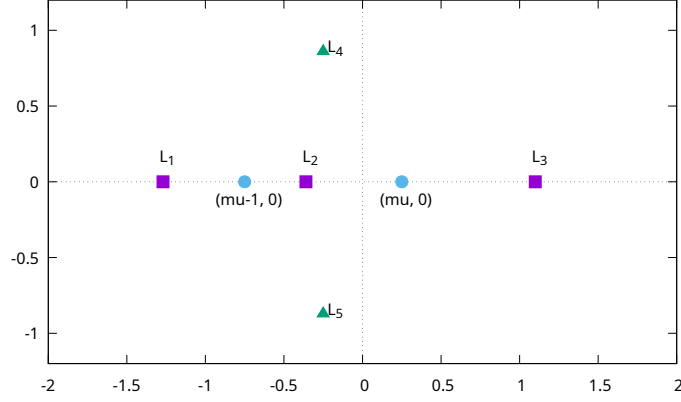
Figure 1.1: Equilibrium points in the RPC3BP for $\mu = 0.25$.

$\Sigma = \{q_y = p_x = q_x - p_y = 0\}$. Their asymptotic q_x coordinate when the mass parameter is small, is given by

$$L_{1,x} = -1 - \left(\frac{\mu}{3}\right)^{\frac{1}{3}} - \frac{1}{3}\left(\frac{\mu}{3}\right)^{\frac{2}{3}} + \frac{28}{27}\mu + \mathcal{O}\left(\left(\frac{\mu}{3}\right)^{\frac{4}{3}}\right)$$

$$L_{2,x} = -1 + \left(\frac{\mu}{3}\right)^{\frac{1}{3}} - \frac{1}{3}\left(\frac{\mu}{3}\right)^{\frac{2}{3}} + \frac{26}{27}\mu + \mathcal{O}\left(\left(\frac{\mu}{3}\right)^{\frac{4}{3}}\right)$$

$$L_{3,x} = 1 + \frac{5}{12}\mu - \frac{1127}{20736}\mu^3 + \mathcal{O}(\mu^4),$$

and they are solutions of

$$q_x + \frac{(1-\mu)(\mu - q_x)}{|q_x - \mu|^2} + \frac{\mu(\mu - q_x - 1)}{|q_x - \mu + 1|^2} = 0. \tag{1.5}$$

When one studies the dynamics around an equilibrium point, usually a good enough approximation for a system $\dot{x} = X(x)$ is to consider the linearized system $\dot{x} = \mathrm{D}X(x_0)(x - x_0)$ with $X(x_0) = 0$. If the original system is Hamiltonian, it is not difficult to check that $\operatorname{tr} \mathrm{D}X(x_0) = 0$ and the eigenvalues are either $\lambda, -\lambda \in \mathbb{R}$, $\pm i\omega \in i\mathbb{R}$ or $\pm a \pm ib$. The real non-zero eigenvalues correspond to the so called saddle character, the pure imaginary ones correspond to the center character and the complex ones correspond to a complex-saddle character.

The collinear equilibrium points (L_1, L_2 and L_3) are of type center-saddle and for small values of μ (more precisely $\mu \leq \mu_R = \frac{1}{2}\left(1 - \frac{\sqrt{69}}{9}\right)$) the two triangular ones (L_4 and L_5) are of type center-center (see [Sze68]).

Since L_1, L_2 and L_3 are of type center-saddle, they each have associated a 1D stable and unstable manifolds. The local stable and unstable manifolds

of an hyperbolic (with non-zero eigenvalues) equilibrium point p in a ODE system $\dot{x} = X(x)$ with flow $\phi(t;x)$ are defined as

$$W_{s,\varepsilon}^{loc} = \{x \mid \|\phi(t;x) - p\| < \varepsilon,\ \forall t \geq 0\},$$
$$W_{u,\varepsilon}^{loc} = \{x \mid \|\phi(t;x) - p\| < \varepsilon,\ \forall t \leq 0\}.$$

They satisfy that they have the same regularity as X does. Let $p \in W_{s,u,\varepsilon}^{loc}$, and $E_{s,u} = T_p W_{s,u}^{loc}$, where

$$E_s = \{v \in \mathbb{R}^n \mid DX(p)v = \alpha v,\ \operatorname{Re}\alpha < 0\}$$
$$E_u = \{v \in \mathbb{R}^n \mid DX(p)v = \alpha v,\ \operatorname{Re}\alpha > 0\}$$

are respectively the stable and unstable linear spaces. In fact a well known result (Hartman's theorem) asserts that that the local dynamics are conjugated with the dynamics of $\dot{x} = DX(p)(x - p)$, namely the system behaves locally as a linear ODE.

When these local stable and unstable manifolds are extended by including the orbits backwards and forwards in time respectively, we obtain the so-called global stable and unstable manifolds. When considering these global invariant manifolds, interesting behaviour appears such as Smale's horseshoes which imply the existence of chaos in the system.

The points L_1, L_2, L_4 and L_5 are widely studied mostly due to the astronomical interest. L_4 and L_5 are stable in the Lyapunov sense, that is, for every $\varepsilon > 0$, $\exists \delta$ such that

$$\|\phi(x_0, 0) - L_{4,5}\| < \delta \implies \|\phi(x_0, t) - L_{4,5}\| < \varepsilon \quad \forall t \geq 0.$$

where $\phi(x_0, t) = (q_x(x_0, t), q_y(x_0, t), p_x(x_0, t), p_y(x_0, t))$ is the solution with initial condition $\phi(x_0, 0) = x_0 \in \mathbb{R}^4$.

For this reason, it is common to find objects near them. For instance Trojan and Greek asteroids in the Jupiter-Sun system. The points L_1 and L_2 (and their associated invariant manifolds) have also been studied (for instance the recently launched James-Webb telescope was launched to the point L_1 in the Earth-Sun system). However, the point L_3 being "at the other side" of the big primary, has received somewhat less attention. This thesis will be concerned with the stable and unstable manifolds of the equilibrium point L_3.

1.1 Stable and unstable manifolds of L_3

As already stated, the equilibrium point L_3 is the solution of (1.5) with $q_x > 1$. This equilibrium point is of type center-saddle. In fact, if we

linearize the system, the matrix obtained is

$$A = \begin{pmatrix} 0 & 1 & 1 & 0 \\ -1 & 0 & 0 & 1 \\ U_{xx} & U_{xy} & 0 & 1 \\ U_{xy} & U_{yy} & -1 & 0 \end{pmatrix}$$

with $U = \frac{1-\mu}{\sqrt{(\mu-q_x)^2+q_y^2}} + \frac{\mu}{\sqrt{(\mu-q_x-1)^2+q_y^2}}$ and

$$
\begin{aligned}
U_{xx} = \frac{\partial^2 U}{\partial q_x^2} = & \frac{3(1-\mu)(\mu-q_x)^2}{\left((\mu-q_x)^2+q_y^2\right)^{\frac{5}{2}}} + \frac{3\mu(\mu-q_x-1)^2}{\left((\mu-q_x-1)^2+q_y^2\right)^{\frac{5}{2}}} \\
& - \frac{(1-\mu)(\mu-q_x)}{\left((\mu-q_x)^2+-q_y^2\right)^{\frac{3}{2}}} + \frac{\mu(\mu-q_x-1)}{\left((\mu-q_x-1)^2+q_y^2\right)^{\frac{3}{2}}}
\end{aligned}
$$

$$
U_{xy} = \frac{\partial^2 U}{\partial q_x \partial q_y} = -q_y\left[\frac{3(1-\mu)(\mu-q_x)}{\left((\mu-q_x)^2+q_y^2\right)^{\frac{5}{2}}} + \frac{3\mu(\mu-q_x-1)}{\left((\mu-q_x-1)^2+q_y^2\right)^{\frac{5}{2}}}\right]
$$

$$
\begin{aligned}
U_{yy} = \frac{\partial^2 U}{\partial q_y^2} = & \frac{3(1-\mu)q_y^2}{\left((\mu-q_x)^2+q_y^2\right)^{\frac{5}{2}}} + \frac{3\mu q_y^2}{\left((\mu-q_x-1)^2+q_y^2\right)^{\frac{5}{2}}} \\
& - \frac{1-\mu}{\left((\mu-q_x)^2+-q_y^2\right)^{\frac{3}{2}}} - \frac{\mu}{\left((\mu-q_x-1)^2+q_y^2\right)^{\frac{3}{2}}}.
\end{aligned}
$$

The characteristic polynomial of A is

$$
\begin{aligned}
p(\lambda) &= \lambda^4 + (2 - U_{xx} - U_{yy})\lambda^2 - U_{xy}^2 + U_{xx}U_{yy} + U_{xx} + U_{yy} + 1 \\
&= \lambda^4 + (2 - U_{xx} - U_{yy})\lambda^2 - U_{xy}^2 + (U_{xx}+1)(U_{yy}+1).
\end{aligned}
$$

We use this information to compute the eigenvalues associated with the equilibrium point L_3. It is not hard to check that, for L_3, we have that

$$U_{xx} > 0,\ U_{xy} = 0 \text{ and } U_{yy} < -1. \tag{1.6}$$

We have

$$\lambda^2 = \frac{(U_{xx} + U_{yy} - 2) \pm \sqrt{(2 - U_{xx} - U_{yy})^2 - 4(U_{xx}+1)(U_{yy}+1)}}{2} \in \mathbb{R}$$

and therefore by (1.6), $\lambda_1, \lambda_2 \in \mathbb{R}$ and $\lambda_3, \lambda_4 \in i\mathbb{R}$. Moreover, it can be proven (see for instance [Sze68]) that

$$\lambda_{1,2,3,4} = \{\pm\sqrt{\mu}\rho(\mu), \pm i\omega(\mu)\}, \quad \text{with} \quad \begin{cases} \rho(\mu) = \sqrt{\frac{21}{8}} + \mathcal{O}(\mu) \\ \omega(\mu) = 1 + \frac{7}{8}\mu + \mathcal{O}(\mu^2). \end{cases} \tag{1.7}$$

This implies the existence of a 1d stable manifold and a 1d unstable manifold. Due to the symmetry (1.4), these manifolds have two branches each: one
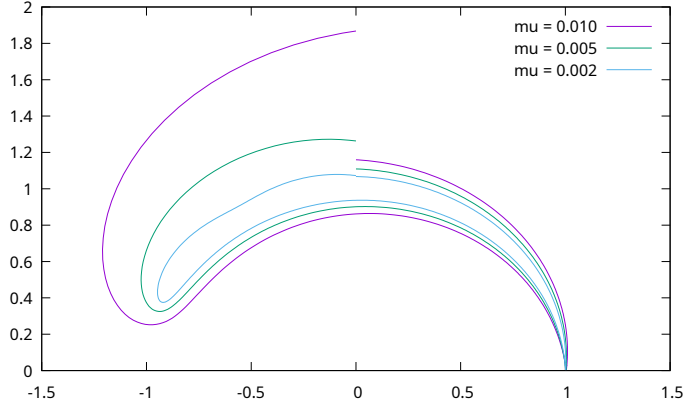
Figure 1.2: Branches $W^{s,+}$ and $W^{s,+}$ of the stable and unstable manifolds of L_3 for different values of μ continued to the Poincaré section Σ.

that circumvents L_4 which we will denote as $W^{s,+}$, $W^{u,+}$ for the stable and unstable manifolds respectively and another one that circumvents L_5 which we will denote as $W^{s,-}$ and $W^{u,-}$. The positive stable branch $W^{s,+}$ is symmetric to $W^{u,-}$ and $W^{s,-}$ is symmetric to $W^{u,+}$. Therefore, one can restrict the study to just the positive branches of the manifolds and the results will follow for the symmetric counterparts.

Let us consider the transversal Poincaré section $\Sigma = \{q_x = 0, q_y > 1\}$ and denote P^u, P^s the first intersections of $W^{u,+}$, $W^{s,+}$ with Σ respectively. (Note that we can consider $\Sigma' = \{q_x = 0\}$ and P^u will be the second intersection between Σ' and $W^{u,+}$). One can visually check (by doing numerical integration) that P^u and P^s are closer and closer as we decrease the values of μ, see Figure 1.2. In fact, in [BGG21a] and [BGG21b] it is proven that

$$\text{dist}_\Sigma(P^u, P^s) = \sqrt[3]{4}\mu^{\frac{1}{3}}e^{\frac{-A}{\sqrt{\mu}}}\left[|\Theta| + \mathcal{O}\left(\frac{1}{\log \mu}\right)\right], \qquad (1.8)$$

where $\Theta \in \mathbb{C}$ is an unknown constant constant, usually called the Stokes constant, and A is given by

$$A = \int_0^{\frac{\sqrt{2}-1}{2}} \frac{2}{1-x}\sqrt{\frac{x}{3(x+1)(1-4x-4x^2)}}\,\mathrm{d}x.$$

So in fact P^u and P^s are exponentially close for small values of μ. This is caused by the difference in magnitude in the eigenvalues of L_3 (1.7). This causes the existence of two times scales, one associated with the "slow saddle dynamics" and another associated with the "fast center dynamics". The dynamics associated with the center behaviour causes that the orbits close to L_3 describe very fast windings around the invariant manifolds, meanwhile

μ	$e^{\frac{-A}{\sqrt{\mu}}}$
$1 \cdot 10^{-4}$	$1.3 \cdot 10^{-8}$
$5 \cdot 10^{-5}$	$1.2 \cdot 10^{-11}$
$1 \cdot 10^{-5}$	$3.8 \cdot 10^{-25}$

Table 1.1: Table comparing the values of μ and $e^{\frac{-A}{\sqrt{\mu}}}$.

the saddle ones cause the orbit to follow (on a very big timescale) the invariant manifolds. That is, the orbits starting near the equilibrium point will perform fast windings around the invariant manifolds while following (somewhat closely) their paths. This behaviour of fast and slow dynamics gives rise to the exponentially small distance described in (1.8).

The goal of this thesis is to numerically check formula (1.8) and to obtain approximations for the value of Θ. As we will see, this numerical computation is very difficult due to cancellations in the computations and the amount of precision required. Indeed the values of μ required to check the formula have to be very small since the error $\mathcal{O}\left(\frac{1}{\log \mu}\right)$ is somewhat big. Since this distance is computed as the difference between two points, that means that we will "lose" the first digits of precision. One can easily estimate the amount of digits that will be dropped as the exponent of $e^{\frac{-A}{\sqrt{\mu}}}$, as this is the order of the distance. In Table 1.1 we see that for $\mu = 5 \cdot 10^{-5}$, at least 11 digits will be lost and for $\mu = 1 \cdot 10^{-5}$, the number goes up to 25.

1.2   Methodology used

Here we will describe the two methodologies we are going to follow to obtain an approximation of Θ.

The first approach will be to work with the original system. This method is described in detail in Chapter 2 but here we will give a brief summary. First we will use the parameterization method described in detail in Section 2.2 to obtain an accurate approximation of $W^{u,+}$ and $W^{s,+}$. Then we will use a numerical integrator that can work with arbitrary precision coupled with a Newton's method to compute with high precision the intersection of the manifolds with Σ and obtain the values of P^{u} and P^{s}. From there, we compute $\mathrm{dist}_{\Sigma}(P^u, P^s)$ for different values μ and obtain different approximation of Θ using

$$\frac{\mathrm{dist}_{\Sigma}(P^{\mathrm{u}}), P^{\mathrm{s}})e^{\frac{A}{\sqrt{\mu}}}}{\sqrt[3]{4}\mu^{\frac{1}{3}}} \approx |\Theta|.$$

The second approach will be more involved and is fully described in Chapter

3. Following [BGG21a] several changes of coordinates are performed in the original system to decouple the center and saddle dynamics in L_3.

More precisely, it is possible (by means of change of variables and singular scalings) to arrive at a Hamiltonian in the form

$$H_0(\lambda, \Lambda, x, y) + H_1(\lambda, \Lambda, x, y; \mu)$$

with $H_1(\cdot, \cdot, \cdot, \cdot; 0) = 0$ and

$$H_0(\lambda, \Lambda, x, y) = -\frac{3}{2}\Lambda^2 + V(\lambda) + i\frac{xy}{\sqrt{\mu}}.$$

In the system associated with H_0, the equilibrium point associated with L_3 is located at the origin and the saddle and center behaviour decoupled at first order. Moreover on the $x = y = 0$ plane, the origin is a saddle with two separatrices (or homoclinic connections). By means of a deep analysis of both

a) the two singularities that appear in the analytical continuation of a time-parameterization of the separatrix and

b) the dominant behaviour of suitable parameterizations of the stable and unstable manifolds close to those singularities,

the so called inner equation (which will be independent of μ) is derived.

Lastly, we study two special solutions of the inner equation that approximate the invariant manifolds near the singularities. The analysis of these solutions will yield a better algorithm to derive values of Θ as it will not require the amount of precision required by the first approach.

Finally, in Chapter 4, we present some conclusions obtained in the project along with some ideas for future work.

Chapter 2

First approach

In this chapter we describe the first and most straightforward approach to the problem. The idea is to compute good approximations of W^{u} and W^{s} near the equilibrium point L_3. Then we choose some points belonging to these approximations and use them as initial condition to, through numerical integration, continue their trajectories until reaching the Poincaré section Σ and calculate P^{u} and P^{s}. Finally we use the computed points $P^{\mathrm{u}}, P^{\mathrm{s}}$ to obtain the value of $\mathrm{dist}(P^{\mathrm{u}}, P^{\mathrm{s}})$ and approximate the value of Θ.

2.1 Computing L_3

The first step to accurately compute the approximations to the invariant manifolds will be to compute the equilibrium point itself. Since L_3 is on the right of the big primary, we seek points of the form

$$P(\xi) = (\mu + \xi, 0, 0, \mu + \xi) \tag{2.1}$$

where ξ is a positive number.

For $P(\xi)$ to be an equilibrium point the following conditions have to be met

$$\begin{cases} \dot{q}_x = p_x + q_y = 0 \\ \dot{q}_y = p_y - q_x = 0 \\ \dot{p}_x = p_y + \frac{(1-\mu)(\mu-q_x)}{\left((\mu-q_x)^2+q_y^2\right)^{\frac{3}{2}}} + \frac{\mu(\mu-q_x-1)}{\left((\mu-q_x-1)^2+q_y^2\right)^{\frac{3}{2}}} = 0 \\ \dot{p}_y = -p_x - q_y \left[\frac{1-\mu}{\left((\mu-q_x)^2+q_y^2\right)^{\frac{3}{2}}} + \frac{\mu}{\left((\mu-q_x-1)^2+q_y^2\right)^{\frac{3}{2}}} \right] = 0. \end{cases}$$

In order to be an equilibrium point, $P(\xi)$, $\xi > 0$ has to satisfy

$$\dot{p}_x = -\mu - \xi + \frac{(1-\mu)\xi}{\xi^3} + \frac{\mu(1+\xi)}{(1+\xi)^3} = 0 \tag{2.2}$$

Since $\xi > 0$, the previous equation (2.2) is equivalent to

$$\mathcal{P}(\xi) = \xi^5 + (\mu + 2)\xi^4 + (2\mu + 1)\xi^3 - (1 - \mu)\xi^2 - 2(1 - \mu)\xi - (1 - \mu)$$
$$= 0. \tag{2.3}$$

The first three coefficients of the polynomial in (2.3) are positive and the second three are all negative, therefore (by Sturm's theorem) the polynomial has at most one real root. Moreover, $P(0) = \mu - 1 < 0$ and $P(1) = 2\mu > 0$ and by Bolzano's theorem, there exists a root in between. So the equation has exactly one real solution.

For each value of μ, we will numerically compute this solution of (2.3) using the Maple routine `solve` with a tolerance of precision $1 \cdot 10^{-250}$ and then recover the coordinates of L_3 using the characterisation (2.1).

2.2   Parameterization method

To compute approximations to W^{u} and W^{s} we will use the celebrated parameterization method [CFL03a; CFL03b; CFL05] that allows us to obtain expansions of the local invariant manifolds of the equilibrium point L_3. This method is much more generic and can be used to obtain approximations to any kind of invariant manifolds, not just the ones associated with equilibrium points (such as invariant tori, periodic orbits, etc.). By applying the method we will obtain good approximations of the local invariant manifold, however these approximations are only good if we stay close to the equilibrium point.

Here we describe the basic ideas of the method in the context of finding invariant manifolds associated with an hyperbolic equilibrium point. More details and particularisations of the method to compute other invariant objects are available in [Har+16].

Assume we have a system $\dot{Z} = G(Z)$ with an equilibrium point Z_0, that is $G(Z_0) = 0$, and that there exists a matrix P (possibly complex) such that

$$P^{-1}\mathrm{D}G(Z_0)P = \begin{pmatrix} \lambda_1 & & & \\ & \lambda_2 & & \\ & & \ddots & \\ & & & \lambda_n \end{pmatrix}, \quad \lambda_j \neq 0.$$

First consider the change of variables $Z = Z_0 + Pz$ to obtain a new system

$$\dot{z} = F(z) = P^{-1}G(Z_0 + Pz). \tag{2.4}$$

where the origin is an equilibrium point and

$$\mathrm{D}F(0) = P^{-1}\mathrm{D}G(Z_0)P = \begin{pmatrix} \lambda_1 & & & \\ & \lambda_2 & & \\ & & \ddots & \\ & & & \lambda_n \end{pmatrix}.$$

We look for parameterizations of the invariant manifold $W(s)$ such that $W(0) = 0$ and W is tangent to the space generated by the eigenvectors associated with the first d eigenvalues of $\mathrm{D}F(0)$ at the origin.

Since we can rearrange the columns of P, we can choose the d first eigenvalues so that W spans the invariant manifold we are interested in. More precisely, we look for a parameterization

$$W \colon U \subset \mathbb{R}^d \to \mathbb{R}^n$$
$$s \mapsto W(s)$$

such that

$$W(s) = \begin{pmatrix} s_1 \\ \vdots \\ s_d \\ 0 \\ \cdots \\ 0 \end{pmatrix} + \mathcal{O}(\|s\|^2).$$

Moreover, we will look for a function $f(s) \colon \mathbb{R}^d \to \mathbb{R}^d$ that describes the dynamics inside the invariant manifold through the equation

$$\dot{s} = f(s).$$

The invariance condition that we want W and f to satisfy is

$$\Phi_t(W(\tilde{s})) = W(\phi_t(\tilde{s})) \tag{2.5}$$

where Φ_t and ϕ_t are the flows of $\dot{z} = F(z)$ and $\dot{s} = f(s)$ respectively. By deriving (2.5) with respect to time t, we obtain

$$F(\Phi_t(W(\tilde{s}))) = \mathrm{D}W(\phi_t(\tilde{s}))f(\phi_t(\tilde{s}))$$

calling $s := \phi_t(\tilde{s})$, we obtain the infinitesimal version of (2.5)

$$F(W(s)) = \mathrm{D}W(s)f(s). \tag{2.6}$$

The aim now is to solve the invariance equation (2.6). First, we will assume that we can write F as a power series in z

$$F(z) = \begin{pmatrix} \lambda_1 z_1 \\ \vdots \\ \lambda_n z_n \end{pmatrix} + \sum_{k \geq 2} F_k(z)$$

where

$$F_k^i(z) = \sum_{k=|l|} F_{k,l}^i z^l, \quad i = 1, \ldots, n$$

is the i-th component of $F_k(z)$, $l = (l_1, \ldots, l_n) \in \mathbb{N}^n$, $|l| = l_1 + \cdots + l_n$ and $z^l = z_1^{l_1} \cdots z_n^{l_n}$.

Similarly, we will search for solutions W and f as power series in s, that is, we will seek W and f of the form

$$W(s) = \begin{pmatrix} s_1 \\ \vdots \\ s_d \\ 0 \\ \vdots \\ 0 \end{pmatrix} + \sum_{k \geq 2} W_k(s), \quad f(s) = \begin{pmatrix} \lambda_1 s_1 \\ \vdots \\ \lambda_d s_d \end{pmatrix} + \sum_{k \geq 2} f_k(s)$$

$$W_k(s) = (W_k^1(s), \ldots, W_k^n(s))^T, \quad f_k(s) = (f_k^1(s), \ldots, f_k^d(s))^T$$

$$W_k^i(s) = \sum_{k=|m|} W_{k,m}^i s^m, \quad i = 1, \ldots, n$$

$$f_k^i(s) = \sum_{k=|m|} f_{k,m}^i s^m, \quad i = 1, \ldots, d$$

where $m \in \mathbb{N}^d$ and we have used the same multi-index notation as before.

One can trivially check that the definitions we have given of W and f satisfy up to first order the invariant equation (2.6), that is,

$$F(W(s)) - \mathrm{D}W(s)f(s) = \begin{pmatrix} \lambda_1 s_1 \\ \vdots \\ \lambda_d s_d \\ 0 \\ \vdots \\ 0 \end{pmatrix} - \begin{pmatrix} \mathrm{Id} \\ 0 \end{pmatrix} \begin{pmatrix} \lambda_1 s_1 \\ \vdots \\ \lambda_d s_d \end{pmatrix} + \mathcal{O}(\|s\|^2) = \mathcal{O}(\|s\|^2).$$

Now, assume that the invariance equation (2.6) is satisfied up to order $k-1$,

namely, we assume there exists $W_1, \ldots, W_{k-1}, f_1, \ldots, f_{k-1}$ such that

$$W^{k-1}(s) = \sum_{j=1}^{k-1} W_j(s) \qquad f^{k-1}(s) = \sum_{j=1}^{k-1} f_j(s)$$

$$F(W^{k-1}(s)) - \mathrm{D}W^{k-1}(s)f^{k-1}(s) = \mathcal{O}(\|s\|^k).$$

We will compute W_k and f_k such that the invariance equation is satisfied up to order k.

Since we are assuming the equation is satisfied up to order $k-1$, and W_k, f_k will not affect those orders, we only need to make sure the equation is satisfied at k-th order. Let us denote by $[\cdot]_k$ the terms of order exactly k and we will skip the dependence on s to lighten up the notation. On the one hand we have

$$
\begin{aligned}
[F(W(s))]_k &= [F(W_{\leq k})]_k = [F(W_{<k} + W_k)]_k \\
&= [F(W_{<k})]_k + \mathrm{D}F(0)W_k \\
&= [F(W_{<k})]_k + \begin{pmatrix} \lambda_1 & & \\ & \cdots & \\ & & \lambda_n \end{pmatrix} \begin{pmatrix} W_k^1 \\ \vdots \\ W_k^n \end{pmatrix} \\
&= \underbrace{[F(W_{<k})]_k}_{(I)} + \underbrace{\begin{pmatrix} \lambda_1 W_k^1 \\ \vdots \\ \lambda_n W_k^2 \end{pmatrix}}_{(II)}.
\end{aligned}
$$

And on the other hand, since $f_0 = 0$

$$
\begin{aligned}
[\mathrm{D}W(s)f(s)]_k &= \sum_{j=0}^{k}[\mathrm{D}W]_j[f]_{k-j} = \sum_{j=0}^{k} \mathrm{D}W_{j+1}f_{k-j} = \sum_{j=0}^{k-1} \mathrm{D}W_{j+1}f_{k-j} \\
&= \mathrm{D}W_1 f_k + \mathrm{D}W_k f_1 + \sum_{j=1}^{k-2} \mathrm{D}W_{j+1}f_{k-j} \\
&= \mathrm{D}W_1 f_k + \mathrm{D}W_k f_1 + \sum_{j=2}^{k-1} \mathrm{D}W_j f_{k-j+1} \\
&= \underbrace{\begin{pmatrix} f_k^1 \\ \vdots \\ f_k^d \\ 0 \\ \vdots \\ 0 \end{pmatrix}}_{(III)} + \underbrace{\mathrm{D}W_k \begin{pmatrix} \lambda_1 s_1 \\ \vdots \\ \lambda_d s_d \end{pmatrix}}_{(IV)} + \underbrace{\sum_{j=2}^{k-1} \mathrm{D}W_j f_{k-j+1}}_{(V)}.
\end{aligned}
$$

Rearranging the terms,

$$(I) + (II) = (III) + (IV) + (V) \iff (IV) - (II) + (III) = (I) - (V).$$

Explicitly, this equation is

$$\mathrm{D}W_k \begin{pmatrix} \lambda_1 s_1 \\ \vdots \\ \lambda_d s_d \end{pmatrix} - \begin{pmatrix} \lambda_1 W_k^1 \\ \vdots \\ \lambda_d W_d^k \end{pmatrix} + \begin{pmatrix} f_k^1 \\ \vdots \\ f_k^d \\ 0 \\ \vdots \\ 0 \end{pmatrix} = \underbrace{[F(W_{<k})]_k - \sum_{j=2}^{k-1} \mathrm{D}W_j f_{k-j+1}}_{R_k}.$$

Using the expansions of W and f and the notation

$$(\lambda^x, m) = \lambda_1 m_1 + \cdots + \lambda_d m_d,$$

we obtain

$$\sum_{k=|m|} \begin{pmatrix} (\lambda^x, m) W_{k,m}^1 s^m \\ \vdots \\ (\lambda^x, m) W_{k,m}^n s^m \end{pmatrix}$$

$$- \sum_{k=|m|} \begin{pmatrix} \lambda_1 W_{k,m}^1 s^m \\ \vdots \\ \lambda_n W_{k,m}^n s^m \end{pmatrix} + \sum_{k=|m|} \begin{pmatrix} f_{k,m}^1 s^m \\ \vdots \\ f_{k,m}^d s^m \\ 0 \\ \vdots \\ 0 \end{pmatrix} = \sum_{k=|m|} \begin{pmatrix} R_{k,m}^1 s^m \\ \vdots \\ R_{k,m}^n s^m \end{pmatrix}$$

or equivalently

$$\sum_{k=|m|} \left\{ \begin{pmatrix} (\lambda^x, m) W_{k,m}^1 \\ \vdots \\ (\lambda^x, m) W_{k,m}^n \end{pmatrix} - \begin{pmatrix} \lambda_1 W_{k,m}^1 \\ \vdots \\ \lambda_n W_{k,m}^n \end{pmatrix} + \begin{pmatrix} f_{k,m}^1 \\ \vdots \\ f_{k,m}^d \\ 0 \\ \vdots \\ 0 \end{pmatrix} \right\} s^m = \sum_{k=|m|} \begin{pmatrix} R_{k,m}^1 \\ \vdots \\ R_{k,m}^n \end{pmatrix} s^m.$$

First, let us solve the equations corresponding to the components that do not involve f, that is the components $i = d+1, \cdots, n$. For those equations we have

$$(\lambda^x, m) W_{k,m}^i - \lambda_i W_{k,m}^i = R_{k,m}^i \implies W_{k,m}^i = \frac{R_{k,m}^i}{(\lambda^x, m) - \lambda_i}$$

as long as $(\lambda^x, m) - \lambda_i \neq 0$. The pairs (m, i) such that

$$(\lambda^x, m) - \lambda_i = 0, \quad i = d + 1, \dots, n$$

are called primary resonances.

For the equations associated with components $i = 1, \dots, d$ we have

$$(\lambda^x, m)W^i_{k,m} - \lambda_i W^i_{k,m} + f^i_{k,m} = R^i_{k,m}.$$

We can choose to solve this equation in two different ways

- In graph style. By setting $W^i_{k,m} = 0$ and then $f^i_{k,m} = R^i_{k,m}$.

- In normal form style. By setting $f^i_{k,m} = 0$ and then $W^i_{k,m} = \frac{R^i_{k,m}}{(\lambda^x,m)-\lambda_i}$.

Notice that for normal form style we require $(\lambda^x, m) - \lambda_i \neq 0$. The pairs such that
$$(\lambda^x, m) - \lambda_i = 0, \quad i = 1, \dots, d$$
are called secondary resonances.

We claim that there are no primary resonances for the unstable or stable invariant manifolds. Indeed, for the unstable invariant manifold, we have $\operatorname{Re} \lambda_i > 0$ for $i = 1, \dots, d$ and $\operatorname{Re} \lambda_j \leq 0$ for $j = d + 1, \dots n$. We have that

$$(\lambda^x, m) - \lambda_j = m_1\lambda_1 + \cdots + m_d\lambda_d - \lambda_j > 0.$$

The same argument can be done with the strictly negative eigenvalues for stable invariant manifold.

By repeating the above procedure and using that the invariance equation is satisfied at first order, we can compute solutions to the invariance equations up to and arbitrary order at least in graph style.

In the case of one dimensional stable and unstable manifolds, there are also no secondary resonances. Indeed

$$(\lambda^x, m) - \lambda_1 = m\lambda_1 - \lambda_1 = (m - 1)\lambda_1 \neq 0$$

as we only have one dimension and $k \geq 2$.

Therefore, in our particular problem we can choose to solve the equation in either graph or normal style. We choose to solve the equation in normal form style as it more numerically stable in general and it provides a bigger domain of applicability.

We will implement a program in Maple that for each value of μ, performs the transformation described in (2.4), then applies the parameterization method

in a normal style to obtain $\tilde{W}^{\mathrm{u,s}}(s)$, parameterizations of the invariant manifolds associated with the transformed system up to a given order. Lastly, it undoes the transformation using

$$W^{\mathrm{u,s}}(s) = L_3 + P\tilde{W}^{\mathrm{u,s}}(s)$$

to obtain an approximation of the positive branch of the stable and unstable invariant manifolds in the RCP3BP. More details about this program and its internals can be found in Section A.1.

2.3   Numerical integration

Now that we have obtained good approximations of the stable and unstable manifolds near the equilibrium point L_3, we extend them until the Poincaré section

$$\Sigma = \{q_x = 0, q_y > 1\}$$

in order to compute their distance.

To that end, we numerically integrate system (1.3) with initial conditions $W^{\mathrm{u,s}}(s)$, for a small value of the parameter s, until reaching the Poincaré section. The choice of s is somewhat important as the error in $W^{\mathrm{u,s}}(s)$ is $\mathcal{O}(|s|^k)$ so the smaller the parameter, the better the approximation. However, one cannot take a infinitely small value of s as when s gets smaller, $W^{\mathrm{u,s}}(s)$ gets closer to the equilibrium point L_3 and integration times grow quickly.

One important aspect of the numerical integration is not to lose significant digits of precision while doing the integration. If we recall, from formula (1.8), we want to compute the distance between the stable and unstable manifolds. Therefore, we need to subtract two quantities that are exponentially close together. In that process we will lose a significant amount of digits of precision and only a few will remain after the subtraction. To this end, all of the computations done with the Taylor integrator had a working tolerance of 10^{-250}.

For that reason, we need a numerical integrator that is capable of working with arbitrary precision. Our choice is to use the Taylor integrator ([JZ05]), a numerical integrator based on Taylor expansions of the vector field, as it comes with support for arbitrary precision computations right away. However, the multiple precision support that comes with Taylor is through the library GMP ([Gt12]). This library is not recommended for working with arbitrary precision floating point numbers as it has a lot of undefined behaviour and inconsistencies. So the library MPFR ([Fou+07]) is the preferred option. To this end, we slightly modify Taylor in order to use this more robust library.

Moreover, in order to compute the points P^u and P^s, some kind of root finding algorithm has to be implemented. This is because P^u and P^s are defined through the intersection with the Poincaré section Σ. And we need to find the exact point where the orbits and Σ coincide.

In our case we implemented Newton's method, since smaller order methods (like the bisection) take too long to achieve the level of accuracy required. To the extreme that with methods that converged slower, the root finding part took (in some cases) more time than the actual integration. More details about the program used to perform these computations and the design choices made can be found in Section A.2.

2.4 Computation of A

In this section we will describe the methodology used to compute the constant A. If you recall, A is defined as

$$A = \int_0^{\frac{\sqrt{2}-1}{2}} \frac{2}{1-x} \sqrt{\frac{x}{3(x+1)(1-4x-4x^2)}}\,\mathrm{d}x.$$

This is an improper integral and computing the value using an ordinary quadratures method will be rather impractical (specially with the amount of precision required). For that reason, to calculate the value of A, we define the function

$$B(t) = \int_0^t \frac{2}{1-x} \sqrt{\frac{x}{3(x+1)(1-4x-4x^2)}}\,\mathrm{d}x.$$

which satisfies the relation $A = B\left(\frac{\sqrt{2}-1}{2}\right)$ and it is the solution of the Cauchy problem

$$\begin{cases} \dot{B}(t) = \frac{2}{1-t} \sqrt{\frac{t}{3(t+1)(1-4t-4t^2)}} \\ B(0) = 0 \end{cases} \tag{2.7}$$

To solve this problem, we use the Taylor integrator mentioned in the previous section and numerically integrate (2.7) until $t = \frac{\sqrt{2}-1}{2}$ to obtain an approximation of

$$A \approx 0.17774383136230954219006694265409$$

with an error of order $1 \cdot 10^{-260}$.

2.5   Summary of the process

We essentially have to repeat the steps described in the previous section for each value of μ to obtain the approximations needed to compute Θ. This is a long and tedious process as it involves a lot of programs and the communication between them has to be done. Although we managed to get a big portion of the process automated, it still required serious amount of manual data processing and copy-pasting between programs. Moreover, parts of the process can take up to two hours due to amount of precision required.

To sum up, the steps we take for each value of μ are the following

1. Compute the value of L_3. This is done using preexisting algorithms that can work with multiple precision.

2. Compute the linearized system for L_3 and compute the matrix P. This is also done using preexisting algorithms that work with multiple precision arithmetic.

3. Perform the parameterization method to obtain approximations of the local stable and unstable manifolds. The implementation details are further explained in Section A.1.

4. Selecting a point in the local stable and unstable manifold that is "close enough" to the equilibrium point so it is closer to the invariant manifold, but far away from L_3 so integration times are somewhat reasonable.

5. Integrate the initial conditions gotten from the previous steps until reaching the Poincaré sections. This part involves two steps: the first (and easy one) is to integrate the initial condition close to the Poincaré section, and the second is to actually compute P^{u} and P^{s}. We use Newton's method to achieve this second part.

6. Computing the approximations of $|\Theta|$. First, we compute the distance between P^{u} and P^{s} from the values obtained in the previous step. Recall that the asymptotic behaviour for this distance is given by

$$\mathrm{dist}_\Sigma(P^{\mathrm{u}}, P^{\mathrm{s}}) = \sqrt[3]{4}\mu^{\frac{1}{3}}e^{\frac{-A}{\sqrt{\mu}}}\left[|\Theta| + \mathcal{O}\left(\frac{1}{\log\mu}\right)\right], \qquad (2.8)$$

and therefore, we solve for Θ to compute the aforementioned approximations

$$\frac{\mathrm{dist}_\Sigma(P^{\mathrm{u}}), P^{\mathrm{s}})e^{\frac{A}{\sqrt{\mu}}}}{\sqrt[3]{4}\mu^{\frac{1}{3}}} \approx |\Theta|. \qquad (2.9)$$

Luckily, we managed to perform the first 4 steps in Maple [Map19] and no data had to be passed around between programs. However, steps 5 and

6 had to be done in C since maple does not support numerical integration with the required amounts of precision, so data have to be transferred from one program to the other. To this end, we design an interface somewhat human-readable and more or less error safe to communicate between the two (More details can be found in Sections A.2 and A.1).

Moreover, to cut the long integration process, at least in half, the integration was done in parallel in separate processes. This supposes and advantage as it cuts in half the time spent integrating, but makes it harder to compute the distance (as the data required now is located in separate processes). Also, in order to debug the part where the distance is computed, one had to wait for the whole integration to finish. For that matter (and due to the amount of bugs caused to some extend by the not so friendly MPFR [Fou+07] interface), we decided to create a separate program that computed the distance (as well as some other metrics to assert that the computations had gone as expected) separately.

In the end, we had to move data from one program to another two times per each value of μ. But thanks to some teaks in the programs and the interfaces we designed, this process was very error-safe and less painful than it normally is to copy data between programs.

2.6 Results

The first thing we do is try to verify the formula (2.8) as this will reassure our computations and give us some confidence that we did not make an error at some point in the process. For that matter, we take logarithms to obtain

$$\log(\text{dist}_\Sigma(P^{\text{u}}, P^{\text{s}})) + \frac{A}{\sqrt{\mu}} = \frac{1}{3}\log(\mu) + C$$

where C is a new constant related to Θ.

With all the values of μ and $\text{dist}_\Sigma(P^{\text{u}}, P^{\text{s}})$, we plot $\log\mu$ against the somewhat artificial value $\log(\text{dist}_\Sigma(P^{\text{u}}, P^{\text{s}})) + \frac{A}{\sqrt{\mu}}$ and fit a line of slope equal to one third. We can observe this plot in Figure 2.1. Concerning this figure some remarks must be done.

Given an order for the parameterization $W^{\text{u,s}}$, some threshold value of μ is achieved, such that for higher values of μ the results obtained are meaningful but they are not for smaller values of μ. As one might expect, as μ decreases, higher orders for the parameterization are required.

Moreover, we can see that as μ gets closer and closer to zero, the values of our independent variable $\log(\text{dist}_\Sigma(P^{\text{u}}, P^{\text{s}})) + \frac{A}{\sqrt{\mu}}$ get closer to the ideal line of slope one third. However, the values keep oscillating back and forth

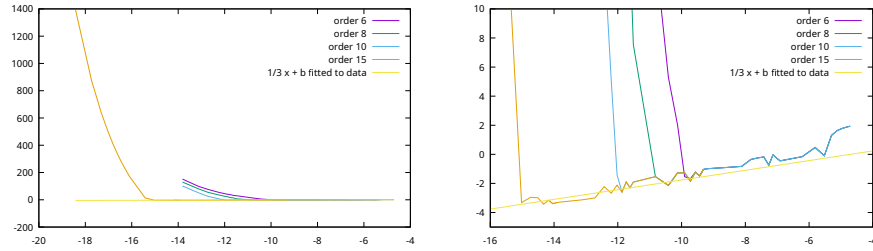Figure 2.1: $\log(\mu)$ against $\log(\mathrm{dist}_\Sigma(P^{\mathrm{u}}, P^{\mathrm{s}})) + \frac{A}{\sqrt{\mu}}$ for different orders of the parameterization method. The figure on the right is a magnified version.
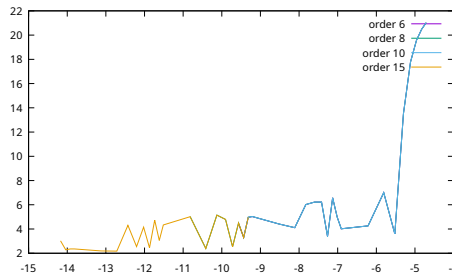

Figure 2.2: $\log \mu$ against the computed value of $|\Theta|$ for different orders of the parameterization method.

around the line in a seemingly random way. This is likely due to the two times scales present in the problem that we talk in Section 1.1. The fact that we are not exactly in the invariant manifold but very close to it, makes us stay trapped in an invariant tube around the actual invariant manifold (this will be the invariant manifold associated to a Lyapunov periodic orbit very close to L_3). This means that upon arriving at the Poincaré section the orbit we are computing has been doing circles around the invariant manifold at a very high speed. This creates some noise (that is practically random due to the difference in time scales) in the calculation of the distance. However, being the distance so small this noise gets greatly amplified giving rise to the errors seen in Figure 2.1.

This same behaviour can bee seen in Figure 2.2, where we have plotted the computed values of Θ given by formula (2.9). As we can see, the values now jump all over the place, this behaviour is similar to the one observed in the previous image but greatly magnified. This is due to the large amplification caused by multiplying by $e^{\frac{A}{\sqrt{\mu}}}$. Precisely this Figure motivates us to apply an alternative method for computing approximations on the value of the constant Θ. This alternative method is described in Chapters 3 and 3.6.

Chapter 3

Inner equation

In this chapter, we follow the approach described in [BGG21a; BGG21b] to attack this problem and derive the inner equation. Please note that we do not intend to present neither a proof nor a complete derivation of the formula but rather some of the key steps and intuitions that lead to it.

The idea is, by means of some changes of variables and singular scalings, to decouple (at first order) the saddle and the center behaviour and write the Hamiltonian of the system as one close to integrable.:w

This close to integrable system is analyzed using singular perturbation theory to obtain the distance distance between manifolds. One of the key tools in this analysis is the so called inner equation from which the constant Θ is defined.

3.1 Changes of coordinates

First, we consider polar coordinates (r, θ, R, G) where $r = \|(q_x, q_y)\|$ and $\theta = \arg(q_x, q_y)$ and R and G are the associated momenta respectively. After performing these changes, the hamiltonian (1.2) can be written as

$$H^{\mathrm{pol}} = H_0^{\mathrm{pol}} + \mu H_1^{\mathrm{pol}}$$

with

$$H_0^{\mathrm{pol}}(r, R, G) = \frac{1}{2}\left(R^2 + \frac{G^2}{r^2}\right) - \frac{1}{r} - G$$

$$\mu H_1^{\mathrm{pol}}(r, \theta; \mu) = \frac{1}{r} - \frac{1-\mu}{\sqrt{r^2 - 2\mu r \cos\theta + \mu^2}} - \frac{\mu}{\sqrt{r^2 - 2(1-\mu)\cos\theta + (1-\mu)^2}}.$$

Note how we have started to write the Hamiltonian as one that is close to integrable by separating the terms that do not depend on μ from the ones

that do depend on μ in the sense that

$$\mu H_1^{\mathrm{pol}}(r, \theta; 0)\Big|_{\mu=0} = 0.$$

When the mass parameter μ is zero, the system becomes a Kepler system (a two body system where the position of one of the bodies is fixed at the origin) and therefore H_0 is in fact integrable. From now on, we will keep this notation where H_0 is the Hamiltonian for $\mu = 0$ and H_1 is the reminder.

In these coordinates, the equilibrium point L_3 satisfies that as $\mu \to 0$

$$(r, \theta, R, G) = (d_\mu, 0, 0, d_\mu^2), \quad \text{with} \quad d_\mu = 1 + \frac{5}{12}\mu + \mathcal{O}(\mu^3).$$

Now we describe Delaunay coordinates. These coordinates (ℓ, L, g, G) are the action-angle variables of the 2-body problem. The variable ℓ is the mean anomaly, g is the argument of the pericenter, L is the square root of the semi-major axis and G is the angular momentum. These coordinates are described by

$$-\frac{1}{2L^2} = \frac{1}{2}\left(R^2 + \frac{G^2}{r^2}\right) - \frac{1}{r} \qquad \theta = f + g \qquad \ell = u - e \sin u,$$

where

$$e = \sqrt{1 - \frac{G^2}{L^2}} \qquad r = L^2(1 - e \cos u)$$

$$\cos f = \frac{\cos u - e}{1 - e \cos u} \qquad \sin f = \frac{\sqrt{1 - r} \sin u}{1 - e \cos u}.$$

We note that e is the eccentricity of the orbit, u is the eccentric anomaly and f is the true anomaly.

The Lagrangian point L_3 satisfies that

$$L = 1 + \mathcal{O}(\mu), \quad G = 1 + \mathcal{O}(\mu), \quad \text{and } \ell + g = 0.$$

Note that this change of coordinates is not well defined when $e = 0$ because the argument of the pericenter g is not well defined as there is no pericenter for a circular orbit. This is a problem since when μ tends to zero, the invariant manifolds get closer and closer to a circular orbit around the big primary. In fact, when $\mu = 0$ we have the Kepler problem and there is a circle of fixed points around the big primary so, in some sense, the invariant manifolds tend asymptotically to a circle of fixed points. For that reason, we want a coordinate system where circular orbits are analytic. To this end, we introduce the Poincaré coordinates.

The Poincaré coordinates are given by

$$\lambda = \ell + g \qquad \eta = \sqrt{L - G}e^{ig} \qquad \xi = \sqrt{L - G}e^{-ig}.$$

Even though these coordinates are defined in terms of Delaunay coordinates, it can be shown that the Poincaré coordinates are analytic when the eccentricity e is zero.

Now we express the system in Poincaré coordinates. One can check that in Poincaré coordinates, the system is Hamiltonian with respect to the symplectic form $d\lambda \wedge dL + id\eta \wedge d\xi$, that is,

$$\dot{\lambda} = \partial_\Lambda H \quad \dot{\Lambda} = -\partial_\lambda H$$
$$\dot{x} = i\partial_y H \quad \dot{y} = -i\partial_x H.$$

Moreover, using the Delaunay coordinates as a middle step, we can define the transformation

$$\phi_{\text{Poi}} \colon (\lambda, L, \eta, \xi) \mapsto (r, \theta, R, G),$$

and the Hamiltonian expressed in Poincaré coordinates becomes

$$H^{\text{Poi}} = H_0^{\text{Poi}} + \mu H_1^{\text{Poi}}$$

with

$$H_0^{\text{Poi}}(L, \eta, \xi) = -\frac{1}{2L^2} - L + \eta\xi \qquad H_1^{\text{Poi}} = H^{\text{pol}} \circ \phi_{\text{Poi}}.$$

Notice that there is no explicit formula for H_1^{Poi}.

In these coordinates, the point L_3 is given by

$$\lambda = 0 \qquad (L, \eta, \xi) = (1, 0, 0) + \mathcal{O}(\mu)$$

and the linearized matrix associated with L_3 is

$$A = \begin{pmatrix} 0 & -3 & 0 & 0 \\ 0 & 0 & 0 & 0 \\ 0 & 0 & i & 0 \\ 0 & 0 & 0 & -i \end{pmatrix} + \mathcal{O}(\mu).$$

As we can see, the center behaviour is found on the coordinates (η, ξ). However, we did not achieve our goal of separating the center and saddle behaviour as in (λ, L) coordinates we see a degenerated equilibrium point. This means that the "saddle behaviour" is "trapped" inside the perturbation.

For that reason, we perform a singular scaling around the circular orbit of radius 1. More precisely, we want that for $\mu = 0$ the new coordinates to be $(\lambda, L, \eta, \xi) = (\lambda, 1, 0, 0)$ which correspond to the coordinates of a circular orbit of radius 1.

To this end, we define

$$\phi_{\mathrm{sc}}\colon (\lambda, L, \eta, \xi) \mapsto (\lambda, \Lambda, x, y), \qquad L = 1 + \delta^2 \Lambda, \quad \nu = \delta x, \quad \xi = \delta y$$

and a time reparameterization $t = \delta^{-2}\tau$, where $\delta^4 = \mu$. The transformed equations are Hamiltonian with Hamiltonian

$$\delta^{-4}\left(H_0^{\mathrm{Poi}} \circ \phi_{\mathrm{sc}}\right) + \left(H_1^{\mathrm{Poi}} \circ \phi_{\mathrm{sc}}\right) \tag{3.1}$$

with respect to the symplectic form $\mathrm{d}\lambda \wedge \mathrm{d}\Lambda + i\mathrm{d}x \wedge \mathrm{d}y$. In addition

$$\delta^{-4}\left(H_0^{\mathrm{Poi}} \circ \phi_{\mathrm{sc}}\right) = \frac{-3}{2}\Lambda^2 + \frac{1}{\delta^4}F_p(\delta^2\Lambda) + \frac{xy}{\delta^2},$$
$$\left(H_1^{\mathrm{Poi}} \circ \phi_{\mathrm{sc}}\right) = V(\lambda) + \mathcal{O}(\delta)$$
$$F_p(z) = \left(\frac{-1}{2(1+z)^2} - (1+z)\right) + \frac{3}{2} + \frac{3}{2}z^2 = \mathcal{O}(z^3)$$
$$V(\lambda) = 1 - \cos\lambda - \frac{1}{\sqrt{2 + 2\cos\lambda}}.$$

In these coordinates, L_3 can be written as

$$\mathcal{L}(\delta) = (0, \mathcal{O}(\delta^2), \mathcal{O}(\delta^3), \mathcal{O}(\delta^3))$$

and the linear part of the flow at L_3 is given by

$$\begin{pmatrix} 0 & -3 & 0 & 0 \\ \frac{-7}{8} & 0 & 0 & 0 \\ 0 & 0 & \frac{i}{\delta^2} & 0 \\ 0 & 0 & 0 & \frac{-i}{\delta^2} \end{pmatrix} + \mathcal{O}(\delta).$$

Now, we have fully separated the saddle and center behaviour at first order (roughly speaking). The center is located in the (x, y) variables and the saddle is in (λ, Λ). We emphasise the different scales in the eigenvalues of L_3. This difference in time scales is the ultimate cause of the exponentially small distance between the invariant manifolds.

Finally, we express Hamiltonian (3.1) as

$$H = H_{\mathrm{p}} + H_{\mathrm{osc}} + H_1$$

with

$$H_{\mathrm{p}}(\lambda, \Lambda) = \frac{-3}{2}\Lambda^2 + V(\lambda), \qquad H_{\mathrm{osc}}(x, y) = \frac{xy}{\delta^2}$$
$$H_1(\lambda, \Lambda, x, y) = (H_1^{\mathrm{Poi}} \circ \phi_{\mathrm{sc}}) + \frac{1}{\delta^4}F_p(\delta^2\Lambda) - V(\lambda).$$

3.2 Preliminary studies

Now that we have managed to separate the saddle and center behaviour at first order, we need to study the distance between the invariant manifolds.

A first approach would be to apply standard Melnikov theory: Let us briefly explain this theory and illustrate it with an example. Assume we have a system

$$\dot{z} = f(z) + \varepsilon g(z, t), \quad z \in \mathbb{R}^2$$

that when $\varepsilon = 0$

- Is Hamiltonian,

- has an hyperbolic saddle at point p_0 and

- has an homoclinic connection $W(t)$ at point p_0,

and the perturbation g is periodic of period T. Assume also that $g(0, t) = 0$. Note that this is not a real restrinction because the point p_0 is an hyperbolic saddle and classical perturbation theory ensures the existance of a periodic orbit ε-close to p_0. We can perform a time-dependent change of variables to put that orbit to the origin.

The idea of Melnikov's theory is to compute a first order approximation of the stable and unstable invariant manifolds by means of the unperturbed homoclinic connection $W(t)$. To that end, it is relatively easy (but quite involved) to prove that the distance between the stable and unstable manifolds of p_0 for the perturbed system at section $\Sigma^{t_0} = \{(x, t) \in \mathbb{R}^2 \times [0, T] \mid t = t_0\}$ (that is, the distance between the invariant manifolds of the Poincaré map) is given by

$$d(t_0) = \frac{\varepsilon M(t_0)}{|f(W(0))|} + \mathcal{O}(\varepsilon^2) \tag{3.2}$$

where $M(t_0)$ is the Melnikov function

$$M(t_0) = \int_{-\infty}^{+\infty} f(W(t)) \wedge g(W(t), t + t_0) \mathrm{d}t.$$

For a more concrete example, consider the Duffing system

$$\begin{cases} \dot{u} = v \\ \dot{v} = u - u^3 + \varepsilon \cos \omega t. \end{cases}$$

For $\varepsilon = 0$, the system has an equilibrium point at $(0, 0)$ and two homoclicic orbits W^+ and W^- which are given by

$$\begin{aligned} W^+(t) &= (\sqrt{2}\operatorname{sech} t, -\sqrt{2}\operatorname{sech} t \tanh t), \\ W^-(t) &= -W^+(t) \end{aligned}$$

The Melnikov function is therefore given by

$$M(t_0) = -\sqrt{2} \int_{-\infty}^{+\infty} \operatorname{sech} t \tanh t \cos(\omega(t + t_0))\mathrm{d}t.$$

First, we write

$$\begin{aligned}
M(t_0) = &- \sqrt{2} \int_{-\infty}^{+\infty} \operatorname{sech} t \tanh t \cos(\omega(t + t_0))\mathrm{d}t \\
= &- \sqrt{2} \int_{-\infty}^{+\infty} \operatorname{sech} t \tanh t \cos \omega t \cos \omega t_0 \mathrm{d}t \\
&+ \sqrt{2} \int_{-\infty}^{+\infty} \operatorname{sech} t \tanh t \sin \omega t \sin \omega t_0 \mathrm{d}t
\end{aligned}$$

Since sech is an odd function and tanh and cos are even, we can conclude that the first integral is equal to zero, that is

$$M(t_0) = \sqrt{2} \int_{-\infty}^{+\infty} \operatorname{sech} t \tanh t \sin \omega t \sin \omega t_0 \mathrm{d}t$$

In order to compute this integral, let us consider

$$\int \operatorname{sech}(z) \tanh(z) e^{i\omega z}\mathrm{d}z.$$

Note that by applying Euler's formula, we get

$$\begin{aligned}
\int \operatorname{sech}(z) \tanh(z) e^{i\omega z}\mathrm{d}z = &\int \operatorname{sech}(z) \tanh(z) \cos \omega z \mathrm{d}z \\
&+ i \int \operatorname{sech}(z) \tanh(z) \sin \omega z \mathrm{d}z
\end{aligned}$$

and therefore, due to the function cos being even, we have that for every $a, b \in \mathbb{R}$ we have that

$$\int_{-a+bi}^{a+bi} \operatorname{sech}(z) \tanh(z) e^{i\omega z}\mathrm{d}z = i \int_{-a+bi}^{a+bi} \operatorname{sech}(z) \tanh(z) \sin \omega z \mathrm{d}z.$$

Consider the contour of the rectangle going from $-R$ to R to $R + i\pi$ to $-R + i\pi$ and back to $-R$. More precisely, consider the paths

$$\begin{aligned}
\gamma_1(t) &= t \\
\gamma_2(s) &= R + s2\pi i \qquad\qquad t \in [-R, R] \\
\gamma_3(s) &= t + 2\pi i \qquad\qquad s \in [0, 1]. \\
\gamma_4(s) &= R + (1 - s)2\pi i
\end{aligned}$$

One can easily check that

$$\lim_{R \to \infty} \int_{\gamma_2, \gamma_4} \operatorname{sech} z \tanh z e^{i\omega z} \mathrm{d}z = 0.$$

Now

$$\int_{-R}^{R} \operatorname{sech}(z) \tanh(z) e^{i\omega z} \mathrm{d}z - \int_{-R+i\pi}^{R+i\pi} \operatorname{sech}(z) \tanh(z) e^{i\omega z} \mathrm{d}z$$
$$= (1 - e^{-2\pi\omega}) \int_{-R}^{R} \operatorname{sech}(z) \tanh(z) e^{i\omega z} \mathrm{d}z.$$

To sum up,

$$\lim_{R \to \infty} \int_{\gamma_1 \vee \gamma_2 \vee \gamma_3 \vee \gamma_4} \operatorname{sech} z \tanh z e^{i\omega z} \mathrm{d}z =$$
$$(1 - e^{-2\pi\omega}) i \int_{-\infty}^{+\infty} \operatorname{sech} z \tanh z \sin \omega z \mathrm{d}z. \tag{3.3}$$

However, since γ_1, γ_2, γ_3 and γ_4 form a closed curve, we can apply the Residue theorem to compute the value of the integral

$$\int_{\gamma_1 \vee \gamma_2 \vee \gamma_3 \vee \gamma_4} \operatorname{sech}(z) \tanh(z) e^{i\omega z} \mathrm{d}z = 2\pi i \operatorname{Res}\left(\operatorname{sech} z \tanh z e^{i\omega z}, \frac{i\pi}{2} \right)$$
$$+ 2\pi i \operatorname{Res}\left(\operatorname{sech} z \tanh z e^{i\omega z}, \frac{3i\pi}{2} \right)$$
$$= 2\pi i \left[e^{\frac{-\pi\omega}{2}} - e^{\frac{-3\pi\omega}{2}} \right]. \tag{3.4}$$

At last, combining (3.3) and (3.4), we get

$$(1 - e^{-2\pi\omega}) i \int_{-\infty}^{\infty} \operatorname{sech}(z) \tanh(z) \sin \omega z \mathrm{d}z = 2\pi i \left[e^{\frac{-\pi}{2}} - e^{\frac{-3\pi}{2}} \right].$$

And we can use this result to obtain an explicit expression for Melnikov's function

$$M(t_0) = \sqrt{2} \pi \omega \operatorname{sech}\left(\frac{\pi\omega}{2} \right) \sin \omega t_0.$$

One can try to use this same methodology for the problem at hand and try to get the analogous of Melnikov function for L_3 and a parameterization of the invariant manifolds. However in the RCP3BP the Melnikov function is exponentially small rendering the approximation in (3.2) effectively useless.

Nonetheless, this example illustrates how the complex poles of a parameterization of the separatrix are very important to understand the distance between the invariant manifolds and for that reason we will dedicate the next section study them.
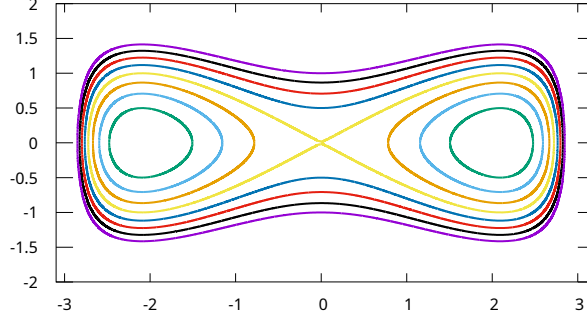
Figure 3.1: Phase portrait of the hamiltonian H_p.

3.3   The Hamiltonian H_{p}

In this section, we study the Hamiltonian H_{p}.

The Hamiltonian system associated with H_{p} has a singularity at $\lambda = \pi$ (associated to the collision with the small primary) and a saddle at the origin with two homoclinic connections. This behaviour is reflected in figure 3.1. The symmetry described in (1.4) translates to a symmetry on the Λ-axis

$$(\lambda, \Lambda) \leftrightarrow (-\lambda, \Lambda),$$

this fact allows us to focus only on one of the separatrices and the result for the other one will follow by symmetry.

Let

$$\sigma \colon \mathbb{R} \to \mathbb{S} \times \mathbb{R}$$
$$t \mapsto (\lambda_h(t), \Lambda_h(t))$$

with $\sigma(0) = (\lambda_0, 0)$, $\lambda_0 \in \left(\frac{2}{3}\pi, \pi\right)$ be a parameterization of the right separatrix.

As stated before, we will like to extend the parameterization of the separatrix into the complex plane. In [BGG21a] it is show that there exists $0 < \beta < \frac{\pi}{2}$ such that σ is analytical in

$$\Pi_{A,\beta} = \{t \in \mathbb{C} \mid |\operatorname{Im} t| < \tan\beta \operatorname{Re} t + A\} \cup \{t \in \mathbb{C} \mid |\operatorname{Im} t| < -\tan\beta \operatorname{Re} t + A\},$$

with

$$A = \int_0^{a_+} \frac{1}{1-x} \sqrt{\frac{x}{3(x+1)(a_+ - x)(x - a_-)}}\, \mathrm{d}x$$

and $a_\pm = \frac{-1}{2} \pm \frac{\sqrt{2}}{2}$. Moreover, σ only has two singularities on $\partial\Pi_{A,\beta}$ at $t = \pm iA$ and Λ_h has only one zero at the closure of $\Pi_{A,\beta}$ at $t = 0$.

The domain is not important aside from the fact that the real and imaginary parts of t can go to infinite and that we know the singularities and the zeroes inside the domain.

3.4 Deriving the inner equation

To measure the distance between the stable and unstable manifolds, we will parameterize them as graphs and "consider the time as a variable". First we will move the equilibrium point to the origin

$$\phi_{\text{eq}} \colon (\lambda, \Lambda, x, y) \mapsto (\lambda, \Lambda, x, y) + \mathcal{L}(\delta).$$

And then we can perform the symplectic change of coordinates

$$\phi_{\text{sep}} \colon (u, w, x, y) \mapsto (\lambda, \Lambda, x, y), \qquad \lambda = \lambda_h(u), \quad \Lambda = \Lambda_h(u) - \frac{w}{3\Lambda_h(u)}.$$

Where we just have taken the easiest change in Λ so that the change is symplectic.

Notice that for the unperturbed system $\dot{u} = 1$ and u represents (to some extend) the time in our new coordinates. Also, since perturbed manifolds can be expressed as a graph, this change is well defined except for $u = 0$.

After the transformation, the Hamiltonian becomes

$$H^{\text{sep}} = H_0^{\text{sep}} + H_1^{\text{sep}}$$

with

$$H_0^{\text{sep}} = w + \frac{xy}{\delta^2}$$
$$H_1^{\text{sep}} = H \circ (\phi_{\text{eq}} \circ \phi_{\text{sep}}) - H_0^{\text{sep}}.$$

The stable and unstable invariant manifolds of H associated with $\mathcal{L}(\delta)$ can be expressed as graphs of "time" u

$$W^{\text{u,s}} = \left\{ \left(\lambda_h(u), \Lambda_h(u) - \frac{w^{\text{u,s}}(u)}{3\Lambda_h(u)}, x^{\text{u,s}}(u), y^{\text{u,s}}(u) \right) + \mathcal{L}(\delta) \right\}$$

with u belonging to appropriate domains. The proof of the existence of $w^{\text{u,s}}$, $x^{\text{u,s}}$ and $y^{\text{u,s}}$ can be found in [BGG21b].

To capture the asymptotic first order of the difference between the manifolds, we need the main terms of the difference at a distance of order δ^2 to the singularities. This is because the other variables (x, y) rotate at frequency $\frac{1}{\delta^2}$. Therefore, we need to be at a distance of around δ^2 to the singularities to avoid the dynamics of (x, y) to interfere.

For this, we derive the inner equation (see [Bal06; BS08]) which captures the first order of the Hamiltonian H^{sep} close to one of the singularities ant it is independent of δ. We seek for a Hamiltonian that can approximate H^{sep} in a neighbourhood of $u = iA$. Note we only focus on the singularity in $u = iA$ but a similar study can be done for $u = -iA$. To this end, we consider $U \in \mathbb{C}$ such that

$$u - iA = \delta^2 U.$$

It can be shown (see [BGG21a]) that for some $\nu > 0$ and $\alpha_+ \in \mathbb{C}$ such that $\alpha_+^3 = \frac{1}{2}$, then

$$\Lambda_h(u) \sim -\frac{2\alpha_+}{3}(u - iA)^{\frac{-1}{3}}$$

$$\text{for} \quad |u - iA| < \nu \quad \text{and} \quad \arg \nu \in \left(\frac{-3\pi i}{2}, \frac{\pi}{2}\right).$$

and

$$w^{\mathrm{u,s}}(iA + \delta^2 U) \sim 3\Lambda_h^2(iA + \delta^2 U) \sim \mathcal{O}\left(\frac{1}{\delta^{\frac{4}{3}} U^{\frac{2}{3}}}\right),$$

$$\frac{x^{\mathrm{u,s}}(iA + \delta^2 U)y^{\mathrm{u,s}}(iA + \delta^2 U)}{\delta^2} \sim \mathcal{O}\left(\frac{1}{\delta^{\frac{4}{3}} U^{\frac{2}{3}}}\right).$$

By symmetry

$$x^{\mathrm{u,s}}(iA + \delta^2 U) \sim \mathcal{O}(\delta^{\frac{1}{3}} U^{\frac{-1}{3}}), \quad y^{\mathrm{u,s}}(iA + \delta^2 U) \sim \mathcal{O}(\delta^{\frac{1}{3}} U^{\frac{-1}{3}}).$$

To capture the first order around $u = iA$ of $w^{\mathrm{u,s}}$, $x^{\mathrm{u,s}}$ and $y^{\mathrm{u,s}}$, we perform the singular symplectic scaling

$$\phi_{\mathrm{in}} \colon (U, W, X, Y) \mapsto (u, w, x, y)$$

given by

$$U = \frac{u - iA}{\delta^2}, \quad W = \delta^{\frac{4}{3}} \frac{w}{2\alpha_+^2}, \quad X = \frac{x}{\delta^{\frac{1}{3}}\sqrt{2}\alpha_+}, \quad Y = \frac{y}{\delta^{\frac{1}{3}}\sqrt{2}\alpha_+},$$

with the time scaling $\tau = \delta^2 t$. As we see below by adding α_+ in the scaling, we also remove the dependence of the nasty coefficients α_+.

Indeed, by applying this change, we obtain

$$H^{\mathrm{in}} = \mathcal{H}(U, W, X, Y) + H_1^{\mathrm{in}}(U, W, X, Y; \delta) \tag{3.5}$$

with $H_1(U, W, X, Y; 0) = 0$ and

$$\mathcal{H}(U, W, X, Y) = W + XY + \mathcal{K}(U, W, X, Y),$$

$$\mathcal{K}(U, W, X, Y) = \frac{-3}{4} U^{\frac{2}{3}} W^2 - \frac{1}{3U^{\frac{2}{3}}} \left(\frac{1}{\sqrt{1 + \mathcal{J}(U, W, X, Y)}} - 1 \right),$$

$$\mathcal{J}(U, W, X, Y) = \frac{4W^2}{9U^{\frac{2}{3}}} - \frac{16W}{27U^{\frac{4}{3}}} + \frac{16}{81U^2} + \frac{4(X + Y)}{9U} \left(W - \frac{2}{3U^{\frac{2}{3}}} \right)$$
$$- \frac{4i(X - Y)}{3U^{\frac{2}{3}}} - \frac{X^2 + Y^2}{3U^{\frac{4}{3}}} + \frac{10XY}{9U^{\frac{4}{2}}}.$$

3.5 Solving the inner equation

In this section, we study the solutions of the inner equation given by the Hamiltonian $\mathcal{H}$ (3.5). The equations of motion of $\mathcal{H}$ are given by

$$\begin{cases} \dot{U} = 1 + \partial_W \mathcal{K} \\ \dot{W} = -\partial_U \mathcal{K} \\ \dot{X} = iX + i\partial_Y \mathcal{K} \\ \dot{Y} = -iY - i\partial_X \mathcal{K} \end{cases} \tag{3.6}$$

And we look for solutions as graphs of "time" u, i.e. solutions of the form

$$Z^{\mathrm{u,s}}(U) = (W^{\mathrm{u,s}}(U), X^{\mathrm{u,s}}(U), Y^{\mathrm{u,s}}(U)).$$

Combining the previous equation with the equations of motion, one can deduce the invariance equation

$$\partial_U Z(U) = \frac{\mathcal{A}Z(U) + f(U, Z(U))}{1 + \partial_W \mathcal{K}(U, Z(U))} \tag{3.7}$$

where

$$\mathcal{A} = \begin{pmatrix} 0 & 0 & 0 \\ 0 & i & 0 \\ 0 & 0 & -i \end{pmatrix}, \quad f(U, Z) = \begin{pmatrix} -\partial_U \mathcal{K}(U, Z) \\ i\partial_Y \mathcal{K}(U, Z) \\ -i\partial_X \mathcal{K}(U, Z) \end{pmatrix}.$$

Since we need uniformity with respect to δ and $U = \delta^{-2}(u - iA)$ then $\operatorname{Re} U \to \pm\infty$ as $\delta \to 0$. We deduce that

$$\lim_{\operatorname{Re} U \to +\infty} Z^{\mathrm{s}}(U) = 0, \quad \lim_{\operatorname{Re} U \to -\infty} Z^{\mathrm{u}}(U) = 0. \tag{3.8}$$

That is, we are interested in solutions that satisfy the aforementioned asymptotic conditions.

It can be shown that (3.7) has analytical solutions for $Z^{\mathrm{u,s}}(U)$ in appropriate complex domains. Moreover there exists a function $\chi = (\chi_1, \chi_2, \chi_3)$ satisfying (3.8) such that

$$\Delta Z(U) = Z^{\mathrm{u}}(U) - Z^{\mathrm{s}}(U) = \Theta e^{-iU}\left((0,0,1) + \chi(U)\right).$$

and

$$\left|U^{\frac{7}{3}}\chi_1(U)\right| \leq b_2, \quad \left|U^2\chi_2(U)\right| \leq b_2, \quad \left|U\chi_3(U)\right| \leq b_2,$$

for some constant $b_2 > 0$. This implies that

$$\Theta = \lim_{\substack{\mathrm{Im}\,U \to -\infty}} \Delta Y(U)e^{iU}. \tag{3.9}$$

In the next Chapter 3.6, we will use this definition of Θ to compute approximations.

3.6   The constant Θ

In this section, we will focus on giving a numerical approximation of the Stokes constant Θ (see (1.8) and (3.9)). In the previous section, we have established a connection between the inner equation and the constant Θ. More precisely in (3.9) we made a connection between the solutions of the invariance equation (3.7) evaluated at the imaginary axis $\{\mathrm{Re}\,U = 0\}$ and Θ, relating them through the limit

$$\Theta = \lim_{\rho \to \infty} \Delta Y(-i\rho)e^{\rho}.$$

Our approach to approximate Θ then will be to compute

$$\Theta_\rho = \left|\Delta Y(-i\rho)\right|e^{\rho} \tag{3.10}$$

for ρ big enough then $\Theta_\rho \approx |\Theta|$.

The first thing we focus in is to obtain a good approximation of $Z^{\mathrm{u,s}}(U)$. To this end, we will look for expansions of $Z^{\mathrm{u,s}}(U)$ as power series in $U^{-\frac{1}{3}}$.

The asymptotic expansion of $Z^{\mathrm{u}}(U)$ as $\mathrm{Re}\,U \to -\infty$ and $Z^{\mathrm{s}}(U)$ as $\mathrm{Re}\,U \to \infty$ are the same. If not, its difference would not be exponentially small as $\mathrm{Im}\,U \to -\infty$. However, this asymptotic expansion is not convergent. This implies that we cannot take higher order expansions to obtain better approximations.

To compute that expansion, we implement a Maple ([Map19]) program that computes the series up to an specified order (since we will want to experiment

with the approximations). More details about the implementation can be found in Section A.3. The first terms of the series are

$$W^{\mathrm{u,s}}(U) = \frac{4}{243 U^{\frac{8}{3}}} - \frac{172}{2187 U^{\frac{14}{3}}} + \mathcal{O}\left(U^{-\frac{20}{3}}\right),$$

$$X^{\mathrm{u,s}}(U) = -\frac{2i}{9 U^{\frac{4}{3}}} + \frac{28}{81 U^{\frac{7}{3}}} - \frac{20i}{27 U^{\frac{10}{3}}} - \frac{16424}{6561 U^{\frac{13}{3}}} + \mathcal{O}\left(U^{-\frac{16}{3}}\right), \quad (3.11)$$

$$Y^{\mathrm{u,s}}(U) = \frac{2i}{9 U^{\frac{4}{3}}} + \frac{28}{81 U^{\frac{7}{3}}} + \frac{20i}{27 U^{\frac{10}{3}}} - \frac{16424}{6561 U^{\frac{13}{3}}} + \mathcal{O}\left(U^{-\frac{16}{3}}\right).$$

In order to compute $\Delta Y(-i\rho)$, we take as initial condition

$$\xi_0^{\mathrm{s}} = \left(\kappa - i\rho, [W^{\mathrm{u}}(\kappa - i\rho)]_p, [X^{\mathrm{u}}(\kappa - i\rho)]_p, [Y^{\mathrm{u}}(\kappa - i\rho)]_p\right),$$

$$\xi_0^{\mathrm{u}} = \left(-\kappa - i\rho, [W^{\mathrm{s}}(-\kappa - i\rho)]_p, [X^{\mathrm{s}}(-\kappa - i\rho)]_p, [Y^{\mathrm{s}}(-\kappa - i\rho)]_p\right),$$

i.e. the power series truncated at order p at points $U = \kappa - i\rho$ for $Z^{\mathrm{s}}(U)$ and $U = -\kappa - i\rho$ for $Z^{\mathrm{u}}(U)$ and some big value of κ. We will take these points as initial conditions for the system of ODEs (3.6) and integrate until the section

$$\Sigma_{\mathrm{in}} = \{(U, W, X, Y) \in \mathbb{C}^4 \mid \operatorname{Re} U = 0\}.$$

3.7 Numerical considerations

As already stated before, we implemented a Maple program to compute the solution of the invariance equation (3.7) as power series truncated at a given order. We will later use this solution as the initial condition for the inner equation.

However, Maple does not have the capability to numerically integrate the system with the amount of accuracy required. Therefore a `C` program had to be developed to integrate the initial conditions until the section Σ_{in}. This supposes an issue because data has to be moved around between programs. To facilitate this task, again, we create an interface that can directly export the power series from Maple so that it can be directly read by the `C` program. This ensures a much more efficient and robust workflow.

This time around however, we needed to integrate a system of complex ODEs. To that end, we had to "trick" the Taylor integrator into thinking he was operating with real numbers. More details about the modification can be found in Section A.4 but in essence, we modify it to use the library MPC [Eng+12] to operate complex numbers in multiple precision. As it is explained in more detail in Section A.4, this modification should not be a problem except it might cause some misscalculations while computing
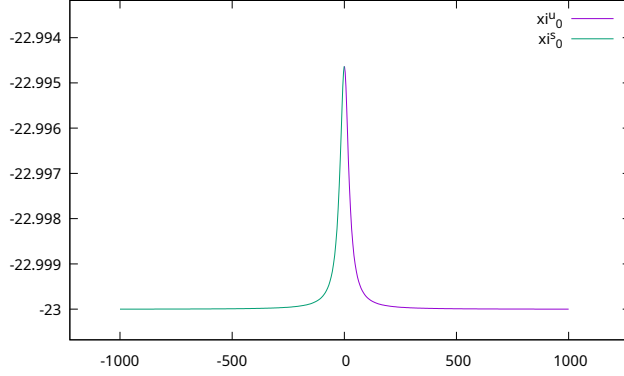
Figure 3.2: Orbits of ξ_0^{u} and ξ_0^{s} for $\kappa = 1000$, $\rho = 23$.

the next integration step. To ensure the tolerance required is achieved, we choose to track the value of the Hamiltonian along the orbit.

The tolerance for is integration is the mentioned 10^{-250} used on all of the integrations throughout this project. In all the experiments we run (including the ones shown in tables 3.1 and 3.2), the Hamiltonian was preserved up to 260 digits of precision, therefore we are certain the integration step is properly computed to satisfy the imposed tolerance.

Note that the imposition of such tolerance makes the integration times be very long and nothing can be done to reduce them (while maintaining the required tolerance). For that matter, we follow the same approach as in the Chapter 2 and decide to add parallelism. This introduces a lot of complexity to a somewhat simple program, however with integration times surpassing the 2 hour mark it was a price that had to be paid.

The last problem to tackle, is that we need to compute the very small difference $\Delta Y(-i\rho)$, that is, we need two evaluate Y at the same point in the $\operatorname{Re} U = 0$ axis.

Note that there is no guarantee that the points ξ_Σ^{u} and ξ_Σ^{s}, the intersection of the orbits of ξ_0^{u} and ξ_0^{s} with Σ_{in}, have the same value of $\operatorname{Im} U$ and according to (3.10). However, looking at the orbits (see Figure 3.2) we can observe a symmetry that is not immediate from the equations but that we will numerically check in the following experiments. That is, we will check that the U component of ξ_Σ^{u} and ξ_Σ^{s} (that we will denote as $\pi_U(\xi_\Sigma^{\mathrm{u}})$ and $\pi_U(\xi_\Sigma^{\mathrm{s}})$) are "close enough" so that we can consider them equal.

3.8   Results

The results obtained are summarised in tables 3.1 and 3.2.

κ	ρ	$\Delta Y(-i\rho)$	$\lvert \pi_U(\xi_\Sigma^{\mathrm{u}}) - \pi_U(\xi_\Sigma^{\mathrm{s}}) \rvert$	e^ρ	Θ_ρ
1000	15	$5.043092 \cdot 10^{-7}$	$1.7 \cdot 10^{-249}$	$3.2422 \cdot 10^6$	1.635062
1000	20	$3.383404 \cdot 10^{-9}$	$2.1 \cdot 10^{-250}$	$4.8218 \cdot 10^8$	1.631402
1000	23	$1.681640 \cdot 10^{-10}$	$5.2 \cdot 10^{-250}$	$9.6926 \cdot 10^9$	1.629951
1000	24	$6.183395 \cdot 10^{-11}$	$1.4 \cdot 10^{-249}$	$2.6353 \cdot 10^{10}$	1.629522
1000	25	$2.273650 \cdot 10^{-11}$	$1.9 \cdot 10^{-249}$	$7.1650 \cdot 10^{10}$	1.629074
1000	30	$1.511938 \cdot 10^{-13}$	$2.6 \cdot 10^{-249}$	$1.0642 \cdot 10^{13}$	1.609096
1000	35	$6.856063 \cdot 10^{-16}$	$2.3 \cdot 10^{-249}$	$1.5804 \cdot 10^{15}$	1.083555
10000	15	$5.043101 \cdot 10^{-7}$	$2.0 \cdot 10^{-249}$	$3.2422 \cdot 10^6$	1.635062
10000	20	$3.383414 \cdot 10^{-9}$	$2.0 \cdot 10^{-249}$	$4.8218 \cdot 10^8$	1.631403
10000	23	$1.681663 \cdot 10^{-10}$	$1.2 \cdot 10^{-249}$	$9.6926 \cdot 10^9$	1.629968
10000	24	$6.183593 \cdot 10^{-11}$	$3.6 \cdot 10^{-249}$	$2.6353 \cdot 10^{10}$	1.629569
10000	25	$2.273835 \cdot 10^{-11}$	$1.1 \cdot 10^{-249}$	$7.1650 \cdot 10^{10}$	1.629203

Table 3.1: Results of the experimentation for various values of κ and ρ and truncated series at order $U^{-\frac{16}{3}}$.

κ	ρ	$\Delta Y(-i\rho)$	$\lvert \pi_U(\xi_\Sigma^{\mathrm{u}}) - \pi_U(\xi_\Sigma^{\mathrm{s}}) \rvert$	e^ρ	Θ_ρ
1000	30	$1.511937 \cdot 10^{-13}$	$4.6 \cdot 10^{-250}$	$1.0643 \cdot 10^{13}$	1.609096
1000	35	$6.856094 \cdot 10^{-16}$	$2.1 \cdot 10^{-250}$	$1.5804 \cdot 10^{15}$	1.083560
10000	30	$1.529456 \cdot 10^{-13}$	$3.2 \cdot 10^{-249}$	$1.0643 \cdot 10^{13}$	1.627734
10000	35	$1.029279 \cdot 10^{-15}$	$2.1 \cdot 10^{-249}$	$1.5804 \cdot 10^{15}$	1.626700
10000	40	$6.938445 \cdot 10^{-18}$	$4.4 \cdot 10^{-249}$	$2.3466 \cdot 10^{17}$	1.628174
10000	45	$5.634902 \cdot 10^{-20}$	$2.4 \cdot 10^{-249}$	$3.4838 \cdot 10^{19}$	1.963118
50000	45	$4.665288 \cdot 10^{-20}$	$4.2 \cdot 10^{-249}$	$3.4838 \cdot 10^{19}$	1.625318

Table 3.2: Results of the experimentation for various values of κ and ρ and truncated series at order $U^{-\frac{25}{3}}$.

The first thing that one notices is that all the values suggest that the first
two digits of the Stokes constant are 1.6. So we can be happy that indeed
Θ seems to be different from zero.

Looking more closely at the data, one can clearly see that for a fixed value
of κ, we can only increment ρ up to a certain point, otherwise we start to
get incorrect results that do not match the expectations. For instance, see
the results obtained for $\kappa = 1000$ and $\rho = 35$. Even increasing the order in
the series in the initial condition, the error is dominated by the small value
of κ.

This behaviour occurs due to the nature of the series (3.11). That series is
divergent, as we have already discussed, and the coefficients grow very fast.
Indeed, the coefficient of $U^{\frac{-38}{3}}$ is already bigger than $9 \cdot 10^4$. This implies
that getting more values of the series does not guarantee an improvement
in the initial approximation. It is clear that to overcome this problem one
has to take bigger values of κ as the error from the series will be dominant
otherwise.

Chapter 4

Conclusions and future work

Although the results obtained seem to suggest that $|\Theta|$ is close (or relatively close) to 1.6, we think that there is not enough evidence to corroborate that. In our opinion, a more involved study has to be made in order to determine the value of the Stokes constant Θ. However, we think that with just a little bit[1] more computing power one can ensure that $\Theta \neq 0$ which is the important thing. The actual value of Θ is not that important apart from being different from zero (otherwise, (1.8) will prove useless). Nonetheless, a more rigorous study doing interval analysis should be done.

Some improvements on the programs can be made like re implementing the parameterization method in a more efficient way or reducing the amount of data that has to be transferred from one program to another. This and other improvements are discussed in Appendix A.

Moreover, the error in the approximations of (3.9) can be bounded as well as the one in the initial approximation of $Z(U)$. Also the numerical methodologies used are well behaved and can be used to perform a proper computer assisted proof to show that $\Theta \neq 0$.

---

[1]This is a joke.

Bibliography

[Bal06]   Inmaculada Baldomá. "The inner equation for one and a half degrees of freedom rapidly forced Hamiltonian systems". In: *Nonlinearity* 19 (June 2006). DOI: 10.1088/0951-7715/19/6/011.

[BGG21a]   Inmaculada Baldomá, Mar Giralt, and Marcel Guardia. "Breakdown of homoclinic orbits to L3 in the RPC3BP (I). Complex singularities and the inner equation". In: (2021). DOI: 10.48550/ARXIV.2107.09942.

[BGG21b]   Inmaculada Baldomá, Mar Giralt, and Marcel Guardia. "Breakdown of homoclinic orbits to L3 in the RPC3BP (II). An asymptotic formula". In: (2021). DOI: 10.48550/ARXIV.2107.09941.

[BS08]   I. Baldomá and Tere M. Seara. "The inner equation for generic analytic unfoldings of the Hopf-zero singularity". In: *Discrete and Continuous Dynamical Systems - B* 10.2&3, September (2008), pp. 323–347.

[CFL03a]   Xavier Cabré, Ernest Fontich, and Rafael de la Llave. "The parameterization method for invariant manifolds. I. Manifolds associated to non-resonant subspaces". In: *Indiana Univ. Math. J.* 52.2 (2003), pp. 283–328. ISSN: 0022-2518. DOI: 10.1512/iumj.2003.52.2245. URL: https://doi.org/10.1512/iumj.2003.52.2245.

[CFL03b]   Xavier Cabré, Ernest Fontich, and Rafael de la Llave. "The parameterization method for invariant manifolds. II. Regularity with respect to parameters". In: *Indiana Univ. Math. J.* 52.2 (2003), pp. 329–360. ISSN: 0022-2518. DOI: 10.1512/iumj.2003.52.2407. URL: https://doi.org/10.1512/iumj.2003.52.2407.

[CFL05]   Xavier Cabré, Ernest Fontich, and Rafael de la Llave. "The parameterization method for invariant manifolds. III. Overview and applications". In: *J. Differential Equations* 218.2 (2005), pp. 444–515. ISSN: 0022-0396. DOI: 10.1016/j.jde.2004.12.003. URL: https://doi.org/10.1016/j.jde.2004.12.003.

[Eng+12]   Andreas Enge et al. *MPC: A C library for the arithmetic of complex numbers with arbitrarily high precision and correct round-*

ing of the result. 2012. URL: https://www.multiprecision.org/mpc/ (visited on 05/30/2022).

[Fou+07] Laurent Fousse et al. "MPFR: A Multiple-Precision Binary Floating-Point Library with Correct Rounding". In: *ACM Trans. Math. Softw.* 33.2 (June 2007), 13–es. ISSN: 0098-3500. DOI: 10.1145/1236463.1236468. URL: https://www.mpfr.org.

[Gt12] Torbjörn Granlund and the GMP development team. *GNU MP: The GNU Multiple Precision Arithmetic Library.* 5.0.5. http://gmplib.org/. 2012.

[Har+16] Àlex Haro et al. *The Parameterization Method for Invariant Manifolds: From Rigorous Results to Effective Computations.* 1st ed. Applied Mathematical Sciences 195. Springer International Publishing, 2016. ISBN: 978-3-319-29660-9.

[JZ05] Angel Jorba and Maorong Zou. "A Software Package for the Numerical Integration of ODEs by Means of High-Order Taylor Methods". In: *Experimental Mathematics* 14 (Jan. 2005), pp. 99–117. DOI: 10.1080/10586458.2005.10128904.

[Map19] Maplesoft, a division of Waterloo Maple Inc.. *Maple.* Version 2019. Waterloo, Ontario, 2019. URL: https://hadoop.apache.org.

[MO17] Kenneth Meyer and Daniel Offin. *Introduction to Hamiltonian Dynamical Systems and the N-Body Problem.* Jan. 2017. ISBN: 978-3-319-53690-3. DOI: 10.1007/978-3-319-53691-0.

[Sze68] Victor Szebehely. "Theory of Orbits: The Restricted Problem of Three Bodies". In: *American Journal of Physics* 36.4 (1968), pp. 375–375. DOI: 10.1119/1.1974535.

Appendix A

Programs developed for the project

A.1 Parameterization method

We choose to implement this method in a very straightforward manner. For the implementation of this and other programs we choose Maple as it was quick and we already have it available, however, any Computer Algebra System that can work with arbitrary precision can be used for the implementation of the programs.

The parameterization method is implemented in a very naive way. This decision turned out to be an error and a great amount of time was spent computing parameterizations. However, it is not trivial to implement the method in a more efficient manner and a more efficient implementation would be enough to be presented as a separate work.

We keep a variable `W` containing the parameterization up to some order k and then, to compute the order $k+1$, we use the command `subs` to substitute the command in the vector field F, we compute the Taylor expansion using the command `mtaylor` and then compute the k-th coefficient and store it in `W`.

We iterate the previous process until the desired order is reached. This core part of the program that implements the parameterization method, can be seen in Figure A.1.

Lastly we choose initial points of the parameterization and output them for the `C` program to use. For this purpose, we choose a value of $s_0 = 1 \cdot 10^{-10}$ and return $W(s_0)$ (the parameterization evaluated in the chosen value) for both the stable and unstable manifold.

```
F := expand(MTM[inv](P)·G1);
W := [s, 0, 0, 0];
for n from 2 to order do
    for i from 1 to 4 do Fi[i] := F[i] : end do:
    for i from 1 to 4 do FSN[i] := subs({z1 = W[1], z2 = W[2], z3 = W[3], z4 = W[4]}, Fi[i]) : end do:
    for i from 1 to 4 do  W[i] := W[i] + (coeff(FSN[i], s^n))/(n·LL[1] − LL[i]) ·s^n : end do:
end do;
WG := expand(Vector(Z0) + P.⟨W[1], W[2], W[3], W[4]⟩) :
```

Figure A.1: Core implementation of the parameterization method

Moreover, we will assert the quality of the parameterization by numerically checking the invariance condition. If you recall, the invariance equation is

$$E_t(s) = \Phi_t(W(s)) - W(\phi_t(s)) = 0$$

so we numerically check that this equation is satisfied for relatively small values of t.

The points $u0$, $s0$ and are the result of evaluating the unstable and stable parameterizations in the small value s_0 are described above. These points serve both as the initial condition for the integration and as values for checking the invariance condition. We compute the points

$$u1 = W\left(s_0 e^{\lambda_+ + t_1}\right), \quad s1 = W\left(s_0 e^{-\lambda_- - t_1}\right).$$

where λ_+ and λ_- are the eigenvalues associated with the positive and negative manifold respectively and t_1 is the value of the time where we check the invariance condition. In our case, we choose $t_1 = 0.5$.

Since we compute the parameterization in normal form style, inside the brackets we have the flow $\phi_{t_1}(t_0)$ and $\phi_{-t_1}(t_0)$ respectively. We output the values of $u1$ and $s1$ alongside t_1 so the C program can perform the comprobation

$$\Phi_{t_1}(u0) = u1, \quad \Phi_{-t_1}(s0) = s1.$$

To communicate the results with the program that performs the numerical integration and that is written in C, we develop an interface consisting on a plain-text file. The interface is designed to be human-readable in order to minimise possible errors.

The first line of the interface consist of a line $n:$ %d that indicates the number of values of μ contained in the file. Then it is followed by $7n$ lines that describe the necessary information for each value of μ. More precisely, the interface for each value of μ is

```
mu: %f
```

```
xL3: %f
t1: %f
u0: %f %f %f %f
u1: %f %f %f %f
s0: %f %f %f %f
s1: %f %f %f %f
```

The first two lines give the value of μ and the position of L_3 for said value of μ. The next line provides the value used for t_1. And the rest of them provide the values of u0, u1, s0 and s1 described above where the coordinates are ordered q_x, q_y, p_x, p_y.

A.2   Numerical integration

As stated previously, the first choice we made after choosing Taylor [JZ05] as our numerical integrator was to migrate from the library GMP to the more robust one MPFR. In fact, in an upcoming update of the numerical integrator, their developers will already migrate official support from the library GMP to MPFR for multiple precision computations.

Apart from this more or less minor change, we implement Newton's method for obtaining precise intersections with the Poincaré section. The methodology is the following: Integrate the initial condition until you cross the Poincaré section (you change sign in q_x). Call q_k the last point before crossing the Poincaré section. We want to find a zero of the function

$$f(t) = \pi_{q_x}(\Phi_t(q_k)).$$

If t_* is a root of $f(t)$, we want to return the point $\Phi_{t_*}(q_k)$.

For finding the root, we take the initial approximation $t_0 = 0$ and iterate the value of t through the Newton process

$$t_j = t_{j-1} - \frac{\pi_{q_x}(\Phi_{t_{j-1}}(q_k))}{\pi_{p_x}(\Phi_{t_{j-1}}(q_k))}$$

since $\dot{q}_x = p_x$.

This program is written to accept files in the form described in the previous section. As such, it accepts several values of μ at the time. This decision is made because integration of both manifolds was taking a big amount of time so computing the unstable and stable manifolds in parallel was the most straightforward manner to reduce that duration. Therefore, once you parallelize and compute the manifolds at the same time, it is not much more difficult to perform the same computations for several values of μ.

This program also takes as an input a destination folder. In this folder it creates a file for every integration, that means two files per each value of μ,

one corresponding to the stable and another one for the unstable manifolds. Each file contains the orbit of the initial value. Each line of the file contains the values q_x, q_y, p_x, p_y, t and the value of the Hamiltonian H computed during the integration. Lastly a new line containing the values for μ, the value of $|\Phi_{\mathtt{t1}}(\mathtt{u0}) - \mathtt{u1}|$ or $|\Phi_{-\mathtt{t1}}(\mathtt{s0}) - \mathtt{s1}|$ (depending on the stable and unstable manifoldsi, see previous section), the difference of the value of the Hamiltonian computed at the point L_3 and at the final point of the integration. Finally, we write the coordinates (q_x, q_y, p_x, p_y) of the final point after applying Newton's method.

After all these files are generated we compute the constant Θ by a simple program as explained in Section 2.5.

A.3 Computation of the solutions of the invariance equation

This program was built to find solutions of the invariance equation

$$\partial_U Z(U) = \frac{\mathcal{A}Z(U) + f(U, Z(U))}{1 + \partial_W \mathcal{K}(U, Z(U))}$$

where $Z(U) = (W(U), X(U), Y(U))^T$.

In order to find the solutions of the above equation, this program uses previous knowledge of the form of the solutions. That is, we know the solutions are of the form

$$W(U) = w_1 U^{\frac{-5}{3}} + w_2 U^{\frac{-8}{3}} + w_3 U^{\frac{-11}{3}} + w_4 U^{\frac{-14}{3}} + \cdots$$
$$X(U) = x_1 U^{\frac{-4}{3}} + x_2 U^{\frac{-7}{3}} + x_3 U^{\frac{-10}{3}} + x_4 U^{\frac{-13}{3}} + \cdots$$
$$Y(U) = y_1 U^{\frac{-4}{3}} + y_2 U^{\frac{-7}{3}} + y_3 U^{\frac{-10}{3}} + y_4 U^{\frac{-13}{3}} + \cdots$$

We consider the function Z up to some fixed order. That is, we write

$$\begin{aligned}
W(U) &= w_1 U^{\frac{-5}{3}} + \cdots + w_k U^{\frac{-3k-2}{3}} \\
X(U) &= x_1 U^{\frac{-4}{3}} + \cdots + x_k U^{\frac{-3k-1}{3}} \\
Y(U) &= y_1 U^{\frac{-4}{3}} + \cdots + y_k U^{\frac{-3k-1}{3}}
\end{aligned} \tag{A.1}$$

and then we compute the series expansion of

$$\frac{\mathcal{A}Z(U) + f(U, Z(U))}{1 + \partial_W \mathcal{K}(U, Z(U))}.$$

in terms of $r = \frac{1}{U}$. Since we want the expansion around $U = \infty$, we have to compute the expansion of the series around $r = 0$. Therefore, we substitute

in the previous equation $U = \frac{1}{r}$ and then use the Maple command `series` to compute the power series in powers of $r^{\frac{1}{3}}$.

As we calculated the right hand side of the equation as a series in r, we have to do the same for the left hand side. To do so, we derive the expressions in (A.1) with respect to U and use the command `subs` to perform the change $U = \frac{1}{r}$.

With that, we have obtained both sides of the equation as power series in r. The only thing left to do is equate the coefficients of the left hand side and the right hand side to obtain a system of equations that can be trivially solved if done in the right way. That is, if one incrementally solves the system, all computations become linear.

Although Maple provides the right answer if we just call the Maple function `solve`, it takes a very long time and is much slower than it should be. The right approach to solve the system is to incrementally solve the system. That is, we consider only the equations associated with the first order and solve them to obtain values for w_1, x_1 and y_1. This is a linear system of equations so its solution is quick and easy to compute. Then consider the equations associated to the second order of the expansion. This system is also linear once the values of w_1, x_1 and y_1 are known. In fact, if we consider the set of equations associated with the k-th order of the expansion. It is a linear system of equations once the values of $w_1, \ldots, w_{k-1}$, $x_1, \ldots, x_{k-1}$ and $y_1, \ldots, y_{k-1}$ are known.

The last thing to do is to export this expansion to be used by the `C` program that is in charge of performing the integration. The interface chosen for this task is the following.

The interface is a file containing 4 lines of plain text

```
n
w1 w2 w3 ... wn
x1 x2 x3 ... xn
y1 y2 y3 ... yn
```

where `n` is the order of the approximation and each coefficient `vi` for `v` $\in \{$`w`, `x`, `y`$\}$ and `i` $= 1, \ldots,$ `n` is in the form

```
num den imag
```

where `num` and `dem` are integers and `imag` $\in \{0, 1\}$. The coefficient is recovered as

$$\text{vi} = \frac{\text{num}}{\text{den}} i^{\text{imag}}.$$

Note that there is no guarantee that the coefficients of the series are pure imaginary or pure real values. However, we have checked that this is the

case for at least the first 100 terms of the series in each variable so this interface is sufficient for every reasonable computation.

A.4   Complex numerical integration

This program takes as an input the values of κ and ρ and a file containing the expansion of the series described in the previous section and outputs the value of Θ and some other values useful for controlling the behaviour of the program.

First, the program divides (forks) himself into two subprograms that will perform the computations for the stable and unstable manifolds.

```
pid_t child_pid = fork();
if (child_pid == 0) {
    /* Child process */
    mpc_set_ui_ui(Z0, kappa, -rho, MPC_RNDNN);
    ...
} else {
    /* Parent process */
    mpc_set_ui_ui(Z0, -kappa, rho, MPC_RNDNN);
    ...
}
```

This allows us to cut integration times in half. Each subprogram substitutes the value of $\kappa - i\rho$ and $-\kappa - i\rho$ corresponding to it. Then this value is used as initial condition for the numerical integration. Lastly, the program joins the two subprocesses back together and computes the value of Θ_ρ, as well as some metrics. More precisely $\Delta Y(-i\rho)$, $\pi_U(\xi_\Sigma^u) - \pi_U(\xi_\Sigma^s)$ and e^ρ.

However, as easy as it sounds, Taylor (as well as most numerical integrators) was not designed to work with complex numbers. To overcome this issue, we decide to trick the program into thinking it was performing integration on real variables. Taylor method has been designed so it is easy to change the underlying arithmetic, that is, Taylor when it has to perform some kind of operations on a number, it calls a function[1] provided by the user.

These functions are all centrally stored in some file and it is easy (but tedious) to change them. For instance, when Taylor has to add two numbers, it calls the function

```
AddMyFloat(r, a, b)
```

This function should compute the sum of values `a` and `b` and store the result

---

[1]It does not call a function but rather it uses a `C` macro that is faster since it is processed at compile time

in `r`. Therefore, what we do is change all of the functions so they work with complex numbers. This is achieved through the library MPC [Eng+12].

This method of tricking Taylor into working with complex numbers should work great as Taylor method is based on taylor expansions and those work the same for real and complex numbers. However, Taylor also performs a step control algorithm in order to be as efficient as possible. This might suppose a problem since we are not using the program as intended.

We choose to ignore this problem and make it easy to check whether it occurs. We monitor the Hamiltonian at each point along the orbit and make sure it is preserved up to the specified tolerance. This will ensure that we are choosing an appropriate step size. In the end, as can be seen in Table 3.1, this method works fine and the step method was chosen correctly.